## General Disclaimer

## One or more of the Following Statements may affect this Document

- This document has been reproduced from the best copy furnished by the organizational source. It is being released in the interest of making available as much information as possible.

- This document may contain data, which exceeds the sheet parameters. It was furnished in this condition by the organizational source and is the best copy available.

- This document may contain tone-on-tone or color graphs, charts and/or pictures, which have been reproduced in black and white.

- This document is paginated as submitted by the original source.

- Portions of this document are not fully legible due to the historical nature of some of the material. However, it is the best reproduction available from the original submission.

Produced by the NASA Center for Aerospace Information (CASI)

ENGINEERING EXPERIMENT STATION
Georgia Institute of Technology
Atlanta, Georgia 303[illegible]

(NASA-CR-120684) A STUDY TO ANALYZE SIX BAND MULTISPECTRAL IMAGES AND FABRICATE A FOURIER TRANSFORM DETECTOR Final Report, 21 Dec. 1973 - 21 Jun. 1975 (Georgia Inst. of Tech.) 87 p HC $4.75 CSCL 14B G3/35

N75-29388

Unclas
33035

FINAL REPORT

PROJECT NO. A-1592

# A STUDY TO ANALYZE SIX BAND MULTISPECTRAL IMAGES AND FABRICATE A FOURIER TRANSFORM DETECTOR

by

R. G. SHACKELFORD

and

J. R. WALSH, JR.


RESEARCH CONTRACT NAS8-30534

21 December 1973 to 21 June 1975

Performed for

NATIONAL AERONAUTICS AND SPACE ADMINISTRATION
George C. Marshall Space Flight Center
Marshall Space Flight Center, Alabama 35812

## ABSTRACT

This report describes the design, development and fabrication of a hybrid optical-digital Fourier transform detector for automatic diffraction pattern analysis. The detector was designed around a concentric ring fiber optic array developed at Georgia Tech under NASA contract NAS8-28215. This array was formed from approximately 89,000 - 3 mil diameter optical fibers which were sorted into 168 concentric rings about a single fiber. All the fibers in each ring were collected into a bundle and terminated into a single photodetector. An optical/digital interface unit consisting of a high level multiplexer and an analog-to-digital amplifier for sampling the outputs of the photodetector - operational amplifier pairs terminating each ring of the fiber optic array was also constructed and is described in this report.

Analysis of the sampled diffraction pattern was accomplished by a digital data processing system, and the software developed for processing Fourier transforms of aerial photographic imagery is described. System parameters relating to the classification of forestry are discussed, and recommendations for improving system performance and utilizing spectral information available from conventional aerial photographs are also included.

TABLE OF CONTENTS

## LIST OF TABLES

## LIST OF FIGURES

LIST OF FIGURES (Continued)

# I. INTRODUCTION

One of the most promising potential applications of coherent optical processing is real time land use classification from a satellite or conventional aircraft platform. Successful development of techniques and equipment for this application would provide land use planners with large scale, up-to-date information which is currently unavailable.

The critical elements in the development of a real time coherent optical land use processing system are the formation of coherent optical images of the terrain in real time, and the extraction of unique spatial signatures for the terrain features of interest. Successful solution of the imaging requirement is well underway with the on-going development of a variety of incoherent-to-coherent imaging devices utilizing liquid crystals, electro-optic single crystals, hot pressed ferroelectric ceramics, and thermoplastics. Techniques for real time exploitation of spatial signatures have not, however, been extensively developed, and the goal of this program has been the design, fabrication and testing of an automatic diffraction pattern analysis system.

Optical processors are capable of performing virtually instantaneous linear transformations on two dimensional data. The Fourier transforming property of a lens can be employed to obtain a spatial signature of any complex image in real time. Some means of sampling and processing this diffraction pattern is necessary if the optical processor is to be used to recognize a particular feature of the image. Matched filters have been employed to perform a cross correlation operation for identification of spatial features. This technique, while effective for many applications, is sensitive to image size and orientation, and registration of the Fourier transform pattern and the filter, and is best suited to the analysis of imagery for which these factors can be precisely controlled.

An alternative procedure for spatial feature analysis is sampling of the diffraction pattern by an array of photodetectors in conjunction with digital processing of the sampled outputs. Even though the digital

processing is a sequential operation, real time analysis is possible in many applications because of the data compression resulting from the optical Fourier transformation, and the relative simplicity of the pattern recognition operations compared with the Fourier transform operation. This combination of optical and digital processing for diffraction pattern analysis represents a hybrid configuration which efficiently utilizes the merits of both processing techniques.

The sampling geometry is an important consideration in a hybrid optical-digital diffraction pattern analyzer. The Fourier transform of a two dimensional object located at any position in the front focal plane of a Fourier transform lens is centered on the optic axis in the back focal plane of the lens. Thus the position of the Fourier transform of an object is independent of the position of that object in the front focal plane, and the sampling operation is always centered on the same space in the back focal plane of the transform lens. Although the Fourier transform is invariant to translation of the object, it is directly dependent on the angular orientation of the object. For this reason, the sampling geometry chosen for the hybrid optical-digital system described in this report consists of optical fibers arranged in concentric rings about a centrally located fiber. The bundle of fibers is oriented with the fiber's axes coincident with to the optical axis, and the ends of the fibers terminated in the diffraction pattern plane. All the fibers in each concentric ring are bundled together and terminated into a single photodetector. Including the central fiber there are approximately 89,000 optical fibers sorted into 168 rings which are terminated into 168 photodetectors. In this manner, each ring in the diffraction pattern plane corresponds to a specific spatial frequency with bandwidth equal to the diameter of the optical fiber.

The output of the photodetectors is a signal which is proportional to the intensity profile of the Fourier transform spatial frequency distribution. This spatial frequency signature is independent of orientation or location of the image feature in the image plane, and can be readily analyzed by a small digital computer. This report describes the development of an automatic hybrid optical-digital diffraction pattern analysis system for

forestry classification from aerial photographs. The design and development of the fiber optic detector array, the optical-digital interface system, and the software employed for analysis are described in the following sections of this report.

## II. SYSTEM CONSIDERATIONS

One of the most important system considerations is the means by which data is introduced into the coherent optical processor. Real time operation will eventually require the use of an incoherent-to-coherent image converter; however, at this time a number of practical considerations discourage their use. Since the goal of this project was the investigation of techniques for automatic diffraction pattern analysis, the superior sensitivity and availability of aerial photographic transparencies provided a compelling basis for their choice as the input medium.

The 70 mm aerial transparencies whose characteristics are listed in Table 1 were provided by MSFC for analysis on this program. These transparencies were first generation copies of aerial photographs which were taken by six Hasselblad cameras. These cameras employed 40 mm wide-angle lenses and were pointed to a common focal spot corresponding to an altitude of 60,000 feet. Spectral coverage from the UV to the infrared was obtained by an appropriate combination of filter and film response characteristics.

The function of the input medium is to generate by laser beam projection a coherent image whose resolution is high enough to result in unique Fourier transform signatures for the objects in question. In this study, the objects were trees, and the desired optical processing operation was the discrimination of coniferous and deciduous classes. This study involved the investigation of techniques for analysis of the optically generated Fourier transform diffraction patterns of forestry images.

The resolution obtained in aerial photography is limited by the quality of the camera's optical system, and the film's inherent resolution, and is also strongly effected by atmospheric conditions, exposure parameters, and processing techniques. The nominal resolving power and exposure index for the different film types employed in the 70 mm aerial photographs are shown in Table 2. The resolving power was determined by procedures outlined in the American National Standards Institute (ANSI) bulletin PH2.33-1969. Where available, the Modulation Transfer Function (MTF) characteristics

Table I. Aerial Photographic Data

Date: May 21, 1971 - Mission 166/177 Tennessee Valley

| SENSOR | Hass 1 | Hass 2 | Hass 3 | Hass 4 | Hass 5 | Hass 6 |
|---|---|---|---|---|---|---|
| FOCAL LENGTH | 40 mm | 40 mm | 40 mm | 40 mm | 40 mm | 40 mm |
| FILM TYPE | 2402 | 2402 | 2424 | SO-356 | 2443 | 2443 |
| FILTER TYPE | 25 | 58 | 89B | 2E | W15 | W15 + 10C |
| ROLL NUMBER | 40 | 41 | 42 | 43 | 44 | 45 |
| ALTITUDE | | 60,000 ft. | | | | |
| FRAMES | 061 → 072: From Tishomingo State Park, Miss. to Summerville, Ga.<br>073 → 084: From Sulphur Springs Station, Ga. to Luka, Miss. | | | | | |

Table II. Aerial Film Characteristics[Δ]

| FILM | TYPE | EXPOSURE INDEX (ASA expect as noted) | RESOLVING POWER (lines/mm - H or L)[†] | MTF (lines/mm at 10%) |
|---|---|---|---|---|
| 2402 | Panchromatic Negative | 80* | 100 - H<br>50 - L | 140 (D-19) |
| 2424 | Infrared Negative | 100* | 100 - H<br>32 - L | 85 (EA-5) |
| 2443 | Infrared False Color | 10* | 63 - H<br>32 - L | 60 (D-19) |
| SO-356(2483) | Ektachrome | 16 | 200 - H<br>100 - L | 140 (E-4) |
| PAN-X | Panchromatic Negative | 32 | 160-- H | - |
| TRI-X | Panchromatic Negative | 250 | 80 - H | - |

* Aerial Exposure Index (not related to ASA)

† H - Test Object Contrast 1000:1, L - Test Object Contrast 1.6:1

Δ Sources for data: Kodak Publications - M-29 Aerial Photography
P-302 Photomicrographic Data
M-61 Kodak Aerial Films and Photographic Plates
P-9 Kodak Plates and Films for Science and Industry
AF-13 Kodak Black and White Films in Rolls

were also listed for comparison. For films used in aerial photography, the film speed is given in terms of the Aerial Exposure Index (AEI) or the Aerial Film Speed (AFS) instead of the ASA index which is usually published for films employed in pictoral photography. A different criterion for speed is required in aerial photography because small changes in luminosity must be detected from ground reflections viewed from altitudes of 50,000 to 100,000 feet sometimes through less than ideal atmospheric conditions. As a result, aerial films are usually exposed and developed for high contrast response, and changes in the slope of the D-Log E characteristic curves become very important in determining the quality of the scene which is photographed. Both the ASA and the AEI and ASF speeds are specified for carefully controlled processing conditions, and the details of their determination are discussed in ANSI bulletins PH 2.34-1969 and PH 2.5-1972.

For comparison, the resolution and approximate ASA speed of some state-of-the-art incoherent-to-coherent image devices are given in Table 3. The equivalent ASA speed parameters were calculated from published sensitivity data [1-4] which can be expected to improve as more sensitive photoconductive materials are developed. It can be seen, however, that the speeds of these devices are much lower than those of the better aerial films, even though their resolving powers are almost competitive. If image intensifiers are employed to overcome the lack of sensitivity of the incoherent-to-coherent converters, the resolution is degraded to the point of being unsatisfactory for high altitude aerial evaluation. A typical CRT system would, for example, provide a 500-2000 line display, whereas a resolution of 6,000 to 14,000 lines is possible with 70 mm aerial film.

The maximum ground resolution of the 70 mm aerial photographs can be calculated from the data of Tables 1 and 2. This calculation is presented in graphical form in Figure 1. The spread in maximum resolution possible for the six 70 mm films is about 7.5 to 24 feet. It should be emphasized that the actual resolution obtainable is highly dependent on the quality of the camera's optical system, and the exposure and processing conditions. Microscopic analysis of enlarged prints obtained from each of the six

Table III. Photographic Characteristics of Incoherent-to-Coherent Imaging Devices

| Device | Sensitivity ($ergs/cm^2$) | Resolution (lines/mm) | Write Wavelength (Å) | Equivalent ASA |
|---|---|---|---|---|
| PROM (ITEK) | 1 | 100 | 4330 | 0.5 |
| OTTO (HUGHES) | 5 | 70 | White | 6 |
| PHOTOTITUS (PHILLIPS) | 100 | 40 | White | 0.3 |
| FERPIC (BELL LABS) | $10^4$ | 40 | White | 0.003 |

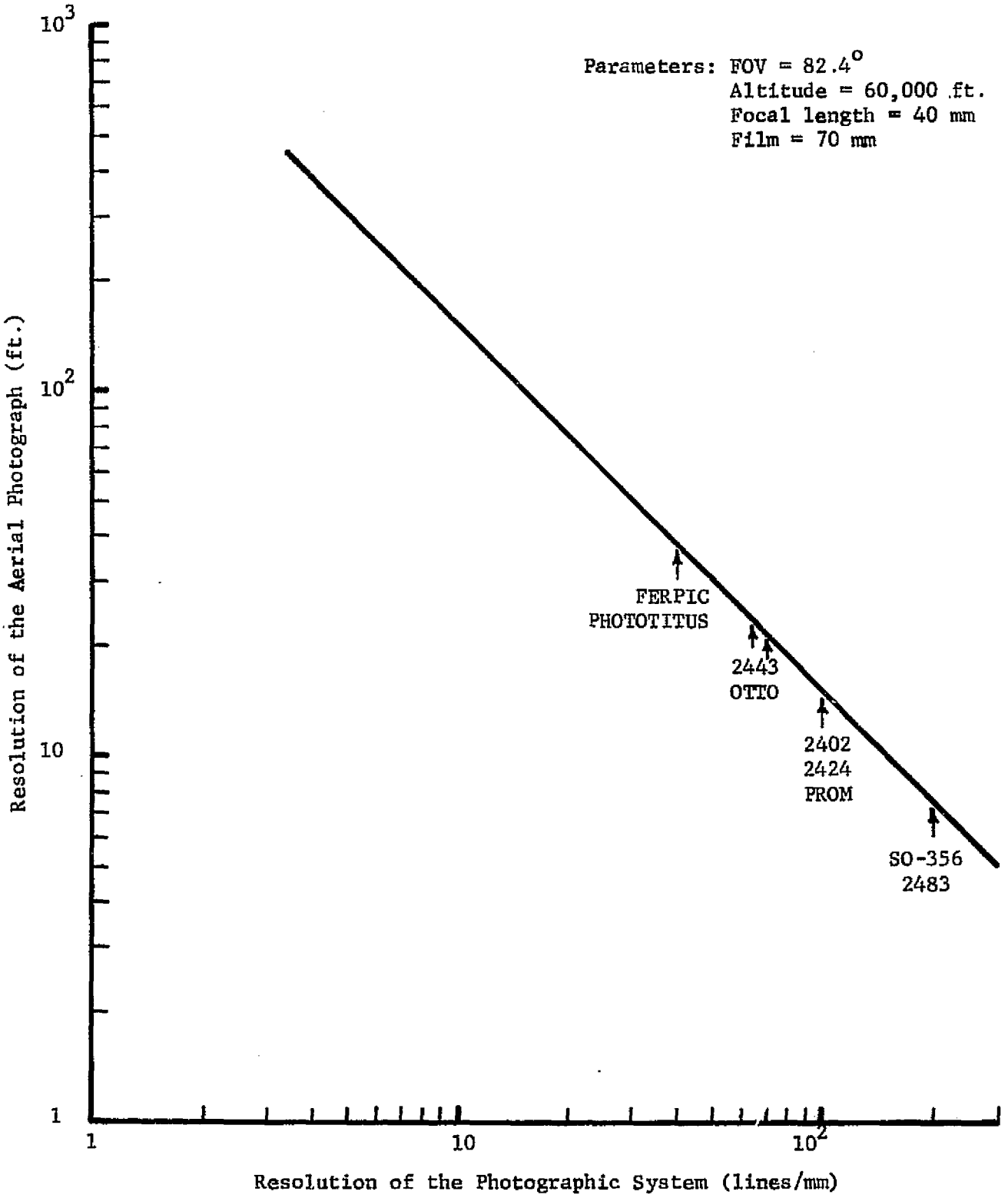


Figure 1. Maximum Calculated Resolution of the 70 mm Aerial Film.

films revealed much lower resolution values than those predicted from Figure 1. Figures 2 and 3 show 19 77 times enlargements of the SO-356 70 mm film compared to the same area on the ground obtained from enlargements of a positive transparency of a 7.5 inch square color infrared aerial plate on unknown emulsion. Both enlargements cover an area of approximately 13,600 ft. x 17,000 ft. on the ground. Although the subjective resolution of the 7.5 inch square plate as determined by microscopic examination was somewhat greater than that of the 70 mm film, the graininess of the later made its apparent resolution appear much worse. The graininess was apparently a result of the high contrast exposure and the subsequent developing process. It was also noted that the exposure, and hence the resolution, varied from the center to the edges of the 70 mm film. This effect could have been caused by the 40 mm wide angle lens. The subjective resolution appeared to be about 15-20 feet for the 7.5 inch square plate, and about 25-30 feet for the 70 mm film. Some loss of resolution and part of the exposure problem could have been a result of the copying process.

Although the quality of the 70 mm aerial film was not as good as one could have hoped for, it was decided to proceed with the optical analysis of this film since MSFC had obtained ground truth data on forestry classification for areas around Huntsville, Alabama and Redstone Arsenal covered by these photographs. It was also recognized that the available spatial information on any aerial photograph taken at an altitude of 60,000 feet would consist primarily of patterns of growth rather than individual tree signatures in view of the limitations imposed by the maximum film resolution. The spatial content of forestry images will also be highly dependent on the season in which the photographs are obtained. During the winter season, the absence of foliage on the deciduous trees should result in changes in spectral and spatial signature which will enhance their classification by optical processing. The 70 mm photographs supplied by MSFC were taken in May, and no enhancement is expected since deciduous trees in the Southeast have usually developed full foliage by this time.

The relationship between the Fourier transform light distribution and the spatial features of the object are also an important system consideration.

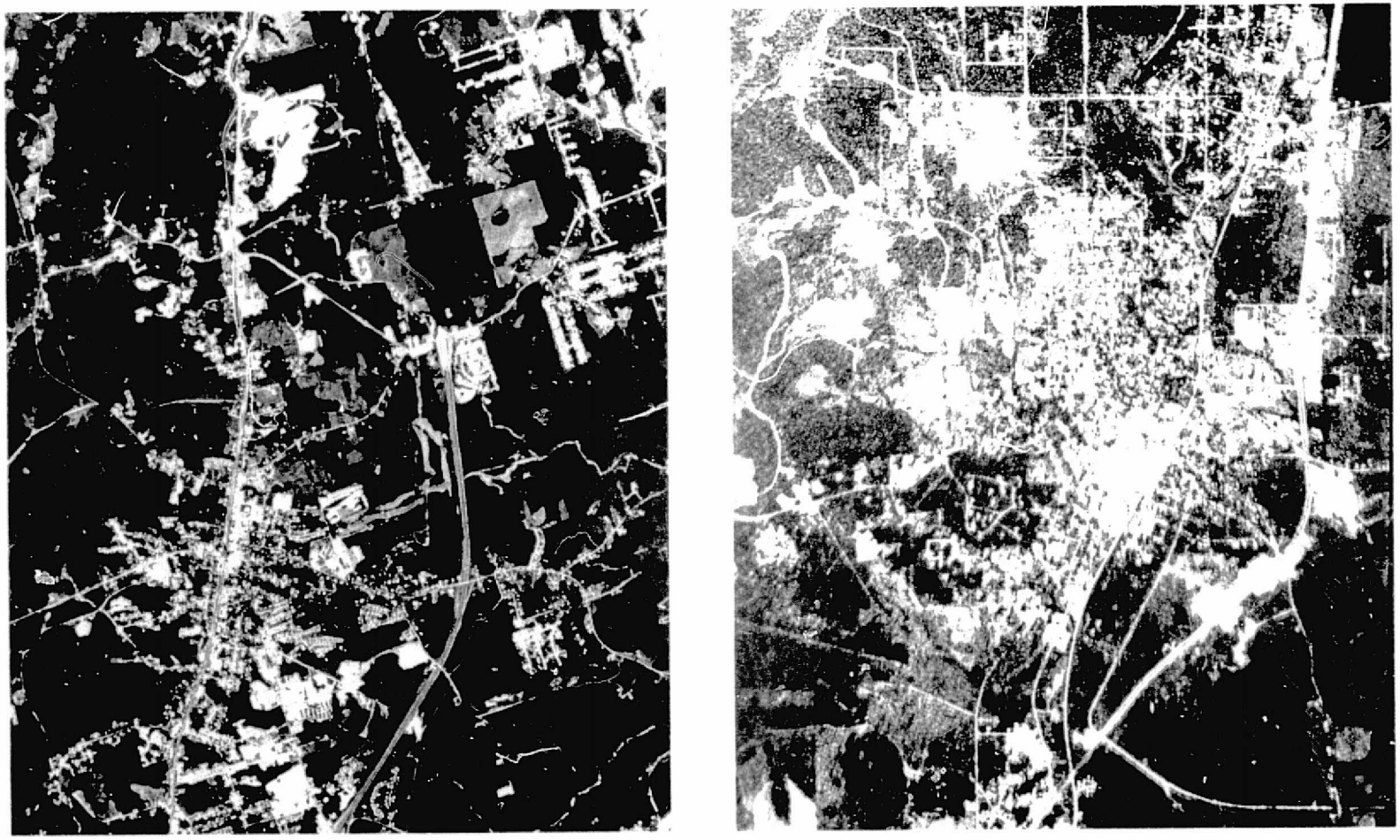

(a) 7.5 inch Square. Color 1R.

(b) 70mm - SO 356.

Figure 2. Comparison of Two Aerial Photographs of an Urban Area (13,600 x 17,000 ft.).

(a) 70mm - SO 356.

(b) 7.5 inch Square. Color 1R.

Figure 3. Comparison of Two Aerial Photographs of Rural Areas (13,600 x 17,000 ft.).

The geometry of the Fourier transform processor is shown in Figure 4. The separation of adjacent maxima of a Fourier transform diffraction pattern corresponding to an object feature of dimension $\Delta X_o$ is approximately $\Delta X_1 = \lambda f/\Delta X_o$, where $\lambda$ is the optical wavelength, and f is the focal length of the Fourier transform lens. The optical processor used in this study employed an argon ion laser source operating on the 488 nm transition, and a Fourier transform lens of 59.89 cm focal length. Setting $\Delta X_1$ equal to the radius of the fiber optic bundle (0.505 in.), the smallest feature which would result in at least one secondary maximum falling on the fiber optic array was found to be 0.023 mm, corresponding to a linear dimension of approximately 30 feet on the ground area covered by the 80 degree FOV from an altitude of 60,000 feet.

The focal length of this lens, which is a highly corrected Fourier transform lens with 488 nm antireflection coatings, is not optimum for the diameter of the fiber optic bundle and the resolution of the image transparency. A focal length of 30 cm would accommodate an image resolution of about 15 feet, and would provide at least three maxima in the diffraction pattern for the measured resolution of the 70 mm aerial photographs. It was, however, necessary to use the existing Fourier transform lens because of the importance of the antireflection coatings in reducing the background light distribution in the diffraction plane. Measurements performed late in the program showed that the transform lens had not been properly coated, and that improved antireflection performance could be obtained by using a helium neon laser at 632.8 nm wavelength. Unfortunately, the highest power helium neon laser available was not compatible with the sensitivity requirements of the fiber optic detector system.

An alternative detector array was also investigated during the coarse of the program. This detector, a Recognition Systems Inc. Model WRD-6400, consisted of a planar silicon ring and wedge array which would have made a low resolution analysis of the aerial photographs possible early in the program while the electronic system for the fiber optics detector was being conceived. Tests were performed using a series of ruled gratings as

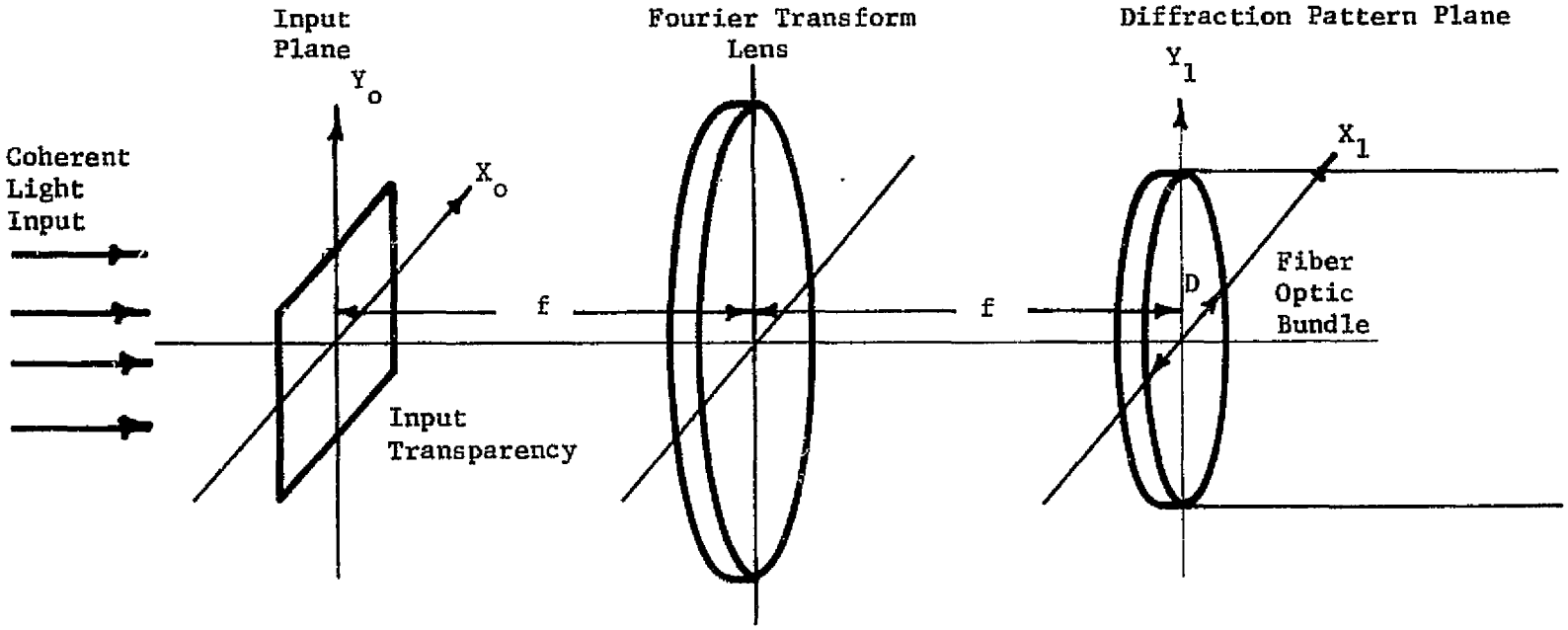


Figure 4. Geometry of the Fourier Transform Optical Processor.

objects to determine the sensitivity and isolation of the array. It was found that the halation effect resulting from scattering of the glass window interfaces limited the dynamic range of this detector system to about 15 dB. It was decided that no useful information concerning the spatial information contained in low contrast aerial forestry images could be obtained with this system. A new RSI detector system, which is not supposed to have the halation problem was ordered, but the order was cancelled after 8 months because RSI was unable to assure delivery.

The third major system consideration involved the conception of effective algorithms for pattern recognition. Since it was not possible apriori to determine the form of the spatial signatures from forestry images, the initial software design goals were focused on providing flexible output data formats, and enhancing the signal-to-noise ratio of the diffraction pattern. To accomplish these goals, both linear and log outputs were provided on variable sampling intervals ranging from a single channel to the entire 169 channels of the detector array. In addition, provisions were made to subtract the background intensity distribution from the diffraction pattern and print out either the corrected or uncorrected values. The details of computer programs required to accomplish these processing operations are described in Section IV of this report.

It was initially planned that analysis of the Fourier transform diffraction patterns of forestry images would be employed as a basis for generating first order algorithms for signature analysis which could be further refined in iterative steps. Difficulties experienced with achieving the hardware performance goals did not, however, leave enough time for this plan to be pursued. Data obtained during the program was found to be useful in generating guidelines for developing pattern recognition algorithms, and these recommendations will be discussed in Section VI of this report.

## III. FIBER OPTIC DETECTOR

The diffraction pattern sampling geometry was determined by the configuration of the concentric ring fiber optic detector array which was chosen as the system detector interface. This array, which was designed and fabricated at EES/Georgia Tech under contract NAS8-28215, consisted of a fiber optic bundle containing approximately 89,000 3 mil optical fibers which were sorted into 168 concentric rings about a single central fiber. On one end of the bundle the fibers were bonded together and polished to a smooth planar surface. The fibers on the end opposite the trunk were sorted into 169 smaller bundles, one for each ring, with the number of fibers per bundle ranging from 1 for the center fiber to approximately 1,060 fibers for the outer ring.

The design concept was to terminate each fiber bundle with a photodetector, and to sample the photodetector outputs with a high speed multiplexer. A preliminary design for the electronic circuitry required to carry out this concept was performed on contract NAS8-28215, but the implementation of the electronic interface was not included in this program. The final design of the electronic interface and the fabrication of the photodiode array was a major part of this program. The details of the fabrication of the photodiode housing and the performance of the detector array are discussed below.

### A. Fabrication Details

To accommodate and align the 169 fiber bundles with the mating photodiodes, a rectangular array of holes of varying diameter was drilled in the mounting plate of the fiber optic detector housing. The diameter of each hole was selected such that the fiber bundle would just fit without compression. The bundles were pulled through the holes from the inside and the bundle lengths adjusted to remove any strains or sharp bends. An epoxy adhesive was then applied to the inside of the mounting plate and the bundles were worked in and out until the epoxy filled the hole. Finally, the bundle was cut with a razor blade flush with the outside surface of the mounting plate. A photograph of the inside of the fiber optic detector housing is shown in Figure 5, and a photograph of the face of the detector with every eleventh ring illuminated from the mounting plate side is shown in Figure 6.

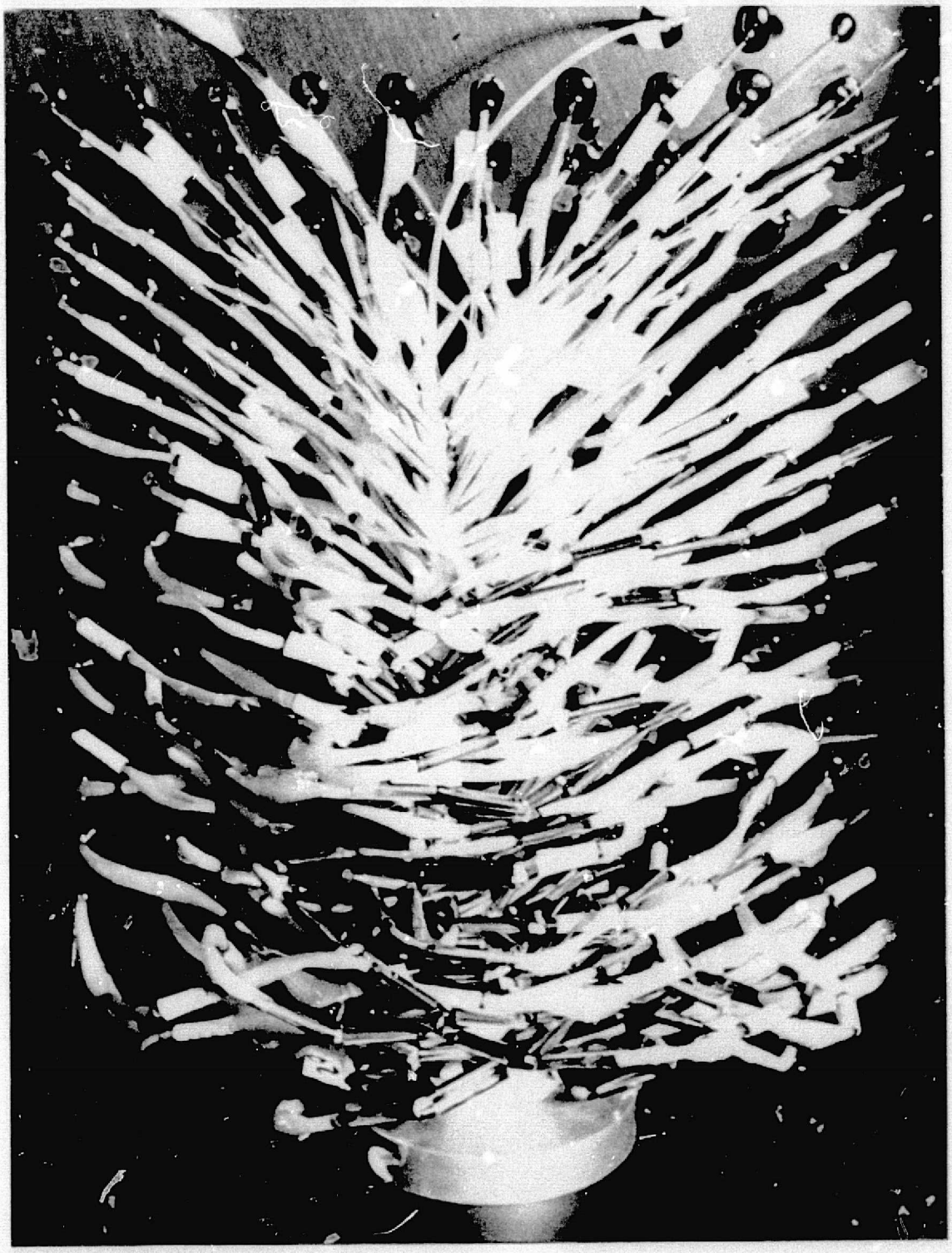

Figure 5. Fiber Optic Detector Housing.

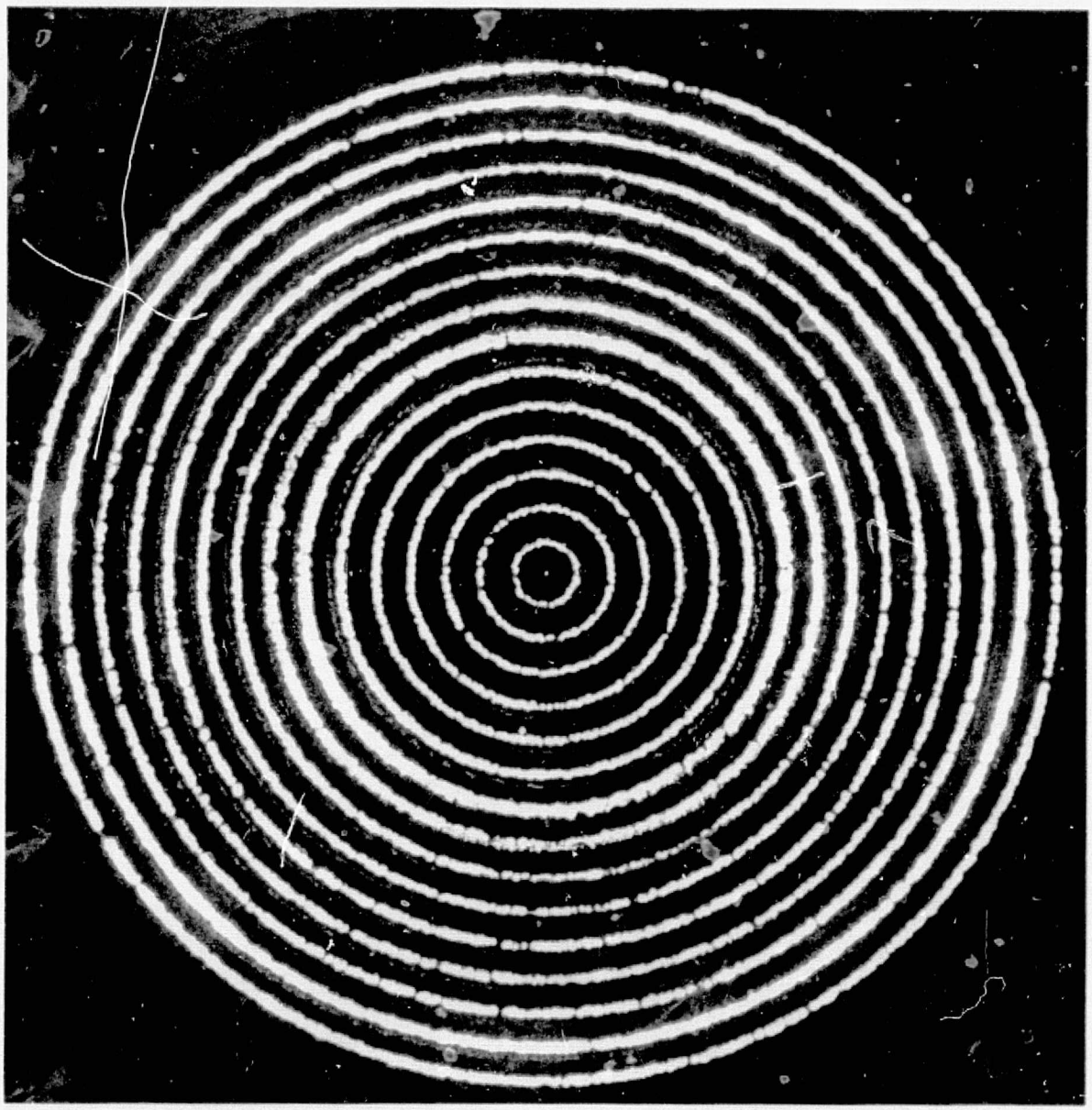

Figure 6. Face of the Fiber Optic Array with Every Eleventh Ring Illuminated on the Mounting Plate.

Correspondence of the ring locations on the face of the array with the locations of the bundle ends on the mounting plate is shown in the layout of Table IV. The rings are assigned numbers in order of increasing radius from the center fiber (ring number 0) to the outer ring (ring number 168). The bundle ends are arranged in a rectangular matrix consisting of 11 columns and 16 rows on the mounting plate. The photodiodes are mounted in a plate with a matching hole pattern as shown in the photograph of Figure 7. Photodiodes with three different active areas were employed, and their assignment to the fiber optic bundles is listed in Table V. The active areas of the photodiodes were selected to be slightly larger than the largest diameter of the fiber bundles to which they were assigned because of the 70 degree radiation beamwidth of the fibers, and the unavoidable separation of the bundle end and the active element of the diode resulting from the diode's mounting configuration. It will be shown in Section V that larger area diodes would have been desireable had they not been economically prohibitive.

In operation, the two mounting plates are placed in contact, and held in proper alignment by machine screws located on the sides of the electronic interface assembly. This assembly will be discussed in detail in Section IV.

## B. Performance

The sampling characteristic of the fiber optic array may be discussed in terms of the power output from each ring of fibers resulting from illumination of the face of the array with a uniform light distribution. This radial distribution function is given by the approximation

$$P(n) \cong 2\pi n I_o A_f L_f L_c, \qquad (1)$$

where $P(n)$ is the power out of the fiber bundle terminating ring number n,

$I_o$ is the input light irradiance at the face of the fiber bundle expressed in $w/cm^2$ (constant over all 169 rings),

$A_f$ is the area of a single 3 mil optical fiber,

$L_f$ is the transmission loss through the length of the fiber,

$L_c$ is the coupling loss at two air-fiber interfaces, and

$2\pi n$ is the number of fibers in ring number n.

Table IV. Fiber Optic Array Layout - Ring Number vs. Row and Column on Mounting Plate.

| Row No. \ Column No. | 1 | 2 | 3 | 4 | 5 | 6 | 7 | 8 | 9 | 10 | 11 |
|---|---|---|---|---|---|---|---|---|---|---|---|
| 1 | 158 | 159 | 160 | 161 | 162 | 163 | 614 | 165 | 166 | 167 | 168 |
| 2 | 147 | 148 | 149 | 150 | 151 | 152 | 153 | 154 | 155 | 156 | 157 |
| 3 | 136 | 137 | 138 | 139 | 140 | 141 | 142 | 143 | 144 | 145 | 146 |
| 4 | 125 | 126 | 127 | 128 | 129 | 130 | 131 | 132 | 133 | 134 | 135 |
| 5 | 114 | 115 | 116 | 117 | 118 | 119 | 120 | 121 | 122 | 123 | 124 |
| 6 | 103 | 104 | 105 | 106 | 107 | 108 | 109 | 110 | 111 | 112 | 113 |
| 7 | 92 | 93 | 94 | 95 | 96 | 97 | 98 | 99 | 100 | 101 | 102 |
| 8 | 81 | 82 | 83 | 84 | 85 | 86 | 87 | 88 | 89 | 80 | 91 |
| 9 | 70 | 71 | 72 | 73 | 74 | 75 | 76 | 77 | 78 | 79 | 80 |
| 10 | 59 | 60 | 61 | 62 | 63 | 64 | 65 | 66 | 67 | 68 | 69 |
| 11 | 48 | 49 | 50 | 51 | 52 | 53 | 54 | 55 | 56 | 57 | 58 |
| 12 | 37 | 38 | 39 | 40 | 41 | 42 | 43 | 44 | 45 | 46 | 47 |
| 13 | 26 | 27 | 28 | 29 | 30 | 31 | 32 | 33 | 34 | 35 | 36 |
| 14 | 15 | 16 | 17 | 18 | 19 | 20 | 21 | 22 | 23 | 24 | 25 |
| 15 | 4 | 5 | 6 | 7 | 8 | 9 | 10 | 11 | 12 | 13 | 14 |
| 16 | | | | | | | | Center | 1 | 2 | 3 |

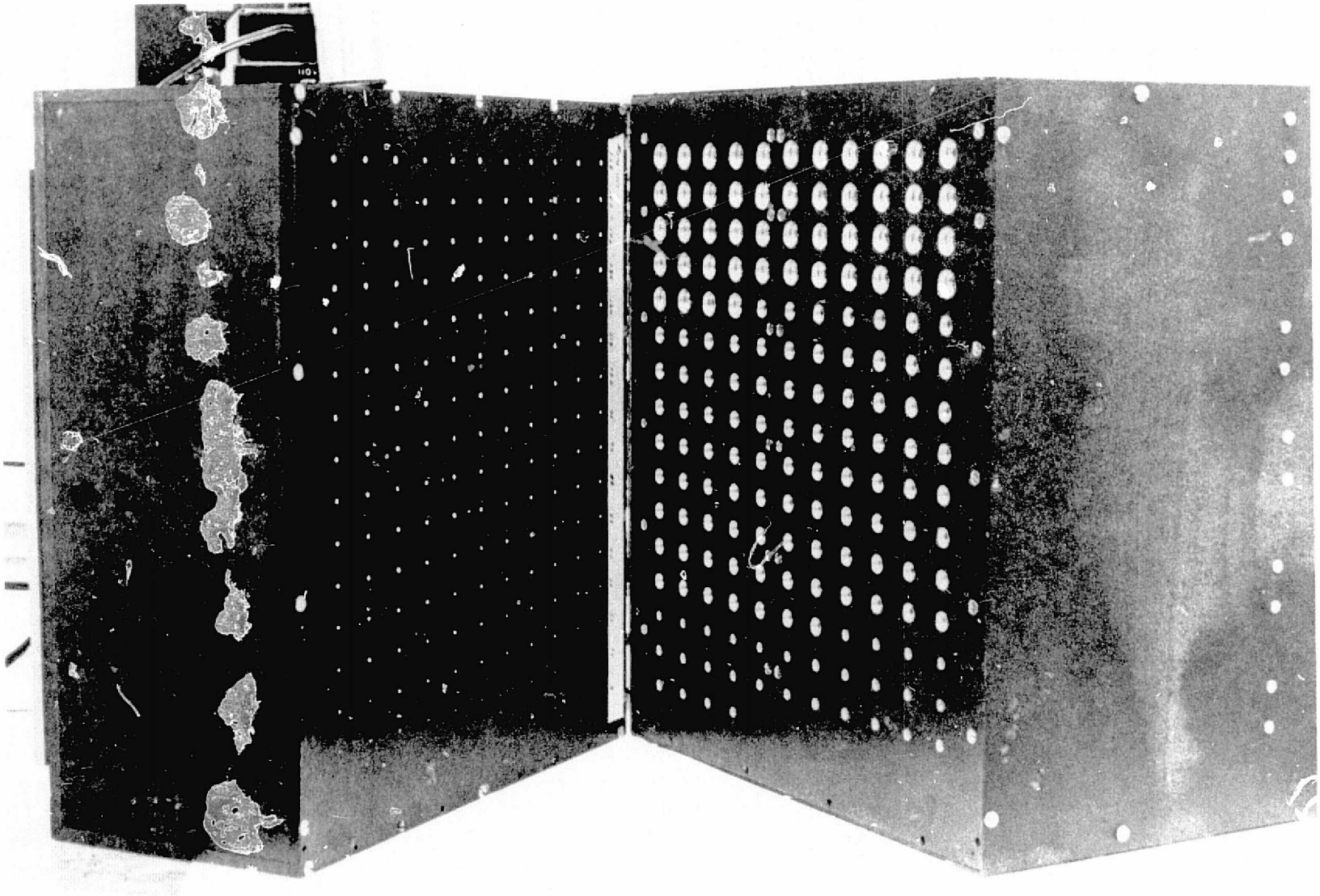

Figure 7. Photograph of the Fiber Optic and Photodiode Mounting Plates.

Table V. Photodiode Characteristics

| Diode Type | Ring Number Assignment | Maximum Bundle Diameter ($cm^2$) | Active Area ($cm^2$) | Sensitivity (volts/μwatt) |
|---|---|---|---|---|
| UDT - 3DP | 0 - 31 | 0.011 | 0.032 | 0.269 |
| UDT - 5DP | 32 - 121 | 0.044 | 0.051 | 0.284 |
| UDT - 6DP | 122 - 168 | 0.061 | 0.203 | 0.235 |

The applicable parameters for the fiber optic detector were:

$$A_f = 4.56 \times 10^{-5} \text{ cm}^2$$

$$L_f = 0.71 \text{ (1 dB/ft x 1.5 ft)}$$

$$L_c = 0.64$$

$$P(n) = 3.65 \times 10^{-7} \, n \qquad (2)$$

The measured characteristic and the calculated characteristic predicted by eqn. (2) are shown in Figure 8. Two illumination sources, one incoherent and the other coherent were employed with identical results. The first distribution was achieved by illuminating a ground glass plate with light from a tungsten lamp, and the variation across the fiber optic detector face was found to be less than 0.5 percent with this configuration. An expanded and spatially filtered argon laser beam was also used to illuminate the ground glass and the resulting light distribution was found to be as uniform as that obtained with the tungsten source. Except for a constant loss factor, good agreement exists between the two curves over most of the detector face; however, the significant departure of the measured points for rings 2 and 3 from the calculated curve strongly suggested that damage had probably occurred to these fiber bundles during the mounting operation. A microscopic analysis of the light distribution on the face of the bundle resulting from illumination of the bundle end array confirmed this suspicion. Figures 9A, 9B, and 9C show photographic enlargements of the light distribution resulting from illumination of one column at a time on the fiber bundle mounting plate containing the fiber bundles connected to rings number 2, 3 and 4. These photographs reveal the individual active fibers in each ring for which light is coupled into the corresponding bundle end. By illuminating one column at a time on the mounting plate, every eleventh ring of the distribution is activated. Missing active fiber locations can be observed for each activated ring of the array, and the resulting variation in active area probably accounts for the variations in the measured radial intensity distribution of Figure 8. It can also be seen that rings 2 and 3 have proportionally many more missing fibers than ring 4 thus accounting for the large observed departures of the measured curve from the calculated curve.

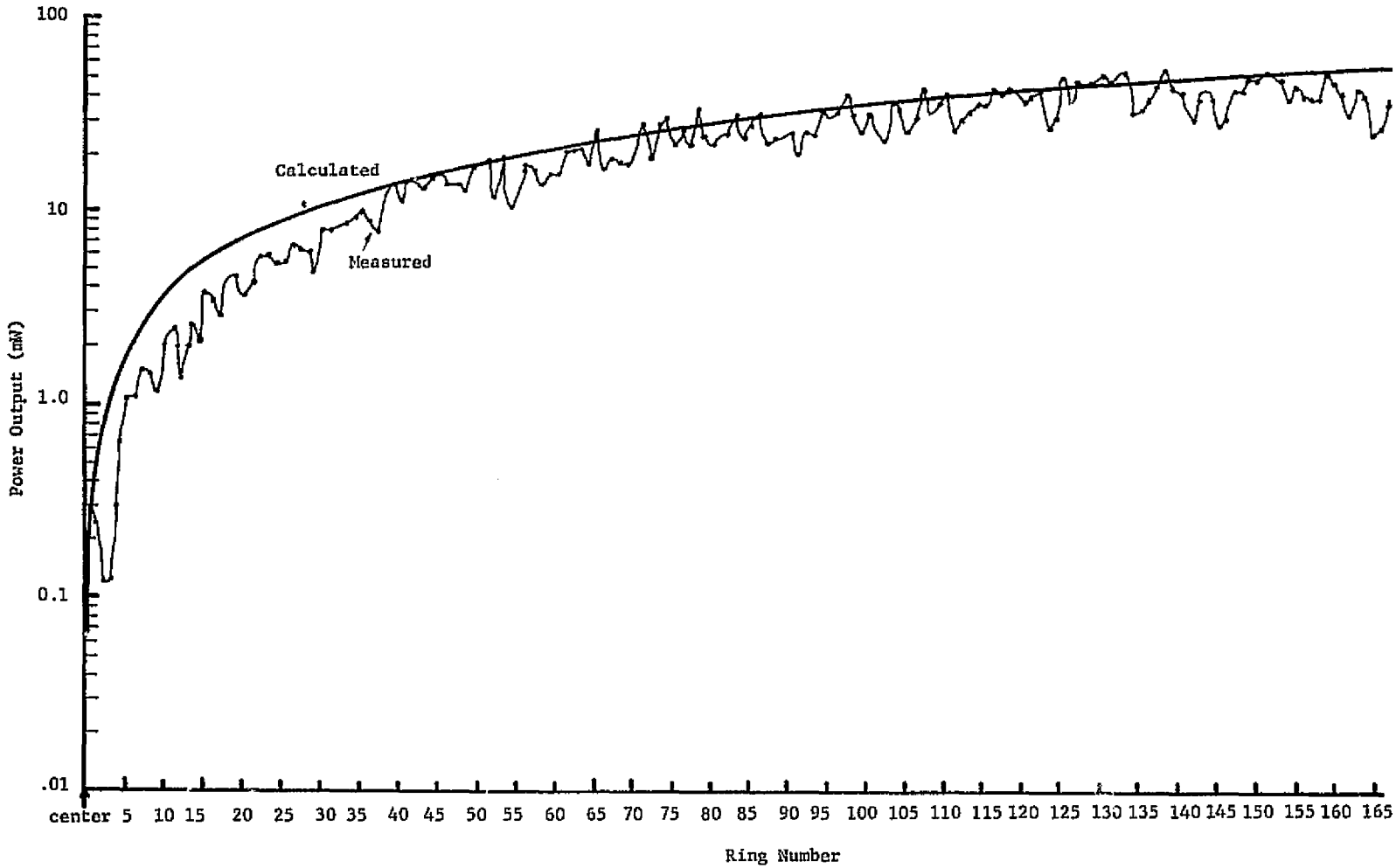


Figure 8. Radial Distribution of Fiber Optic Detector Power Output for Uniform Illumination.

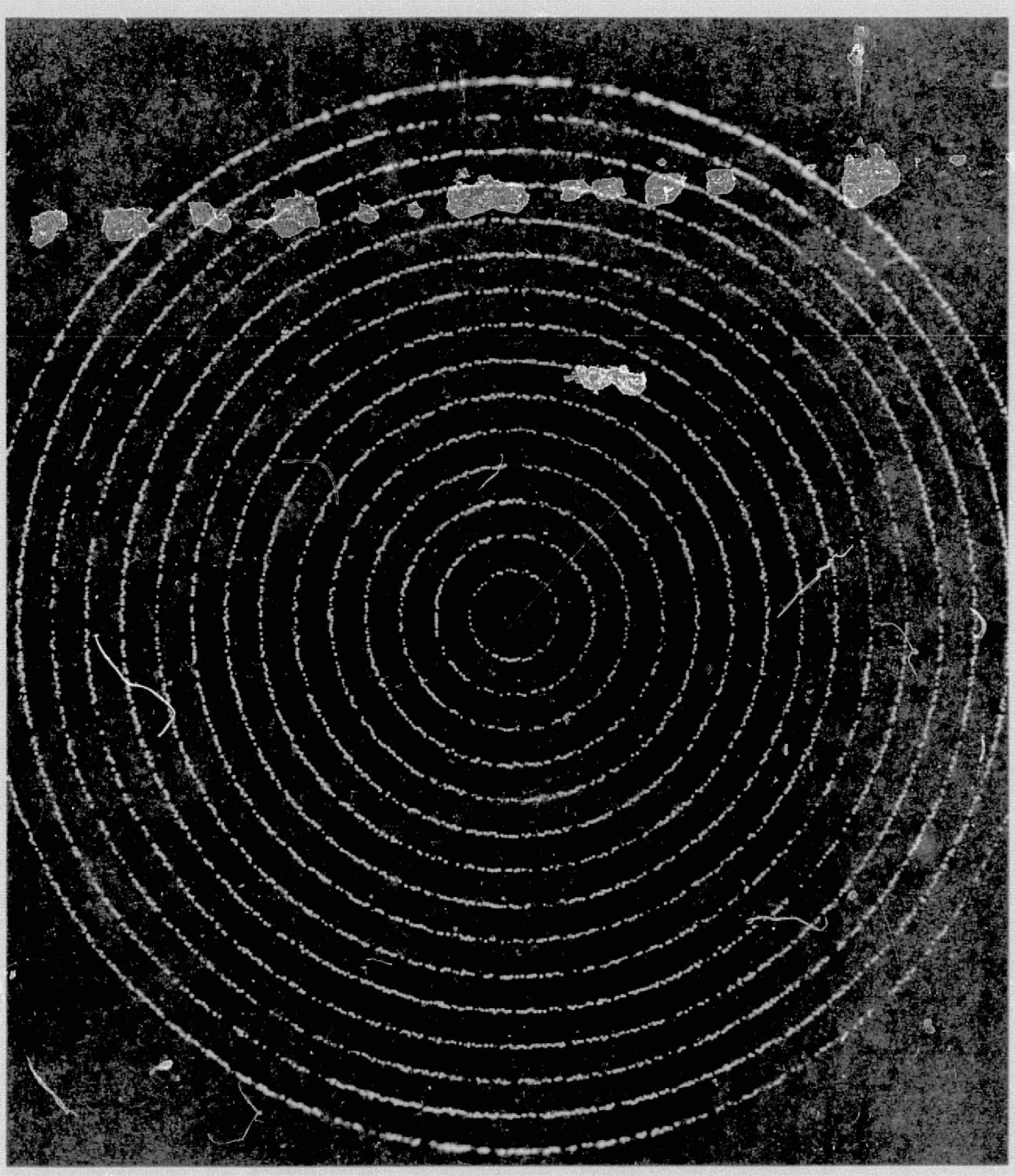

Figure 9A. Fiber Optic Array Light Distribution Resulting From Illumination of Column 10 in the Fiber Bundle Mounting Plate.

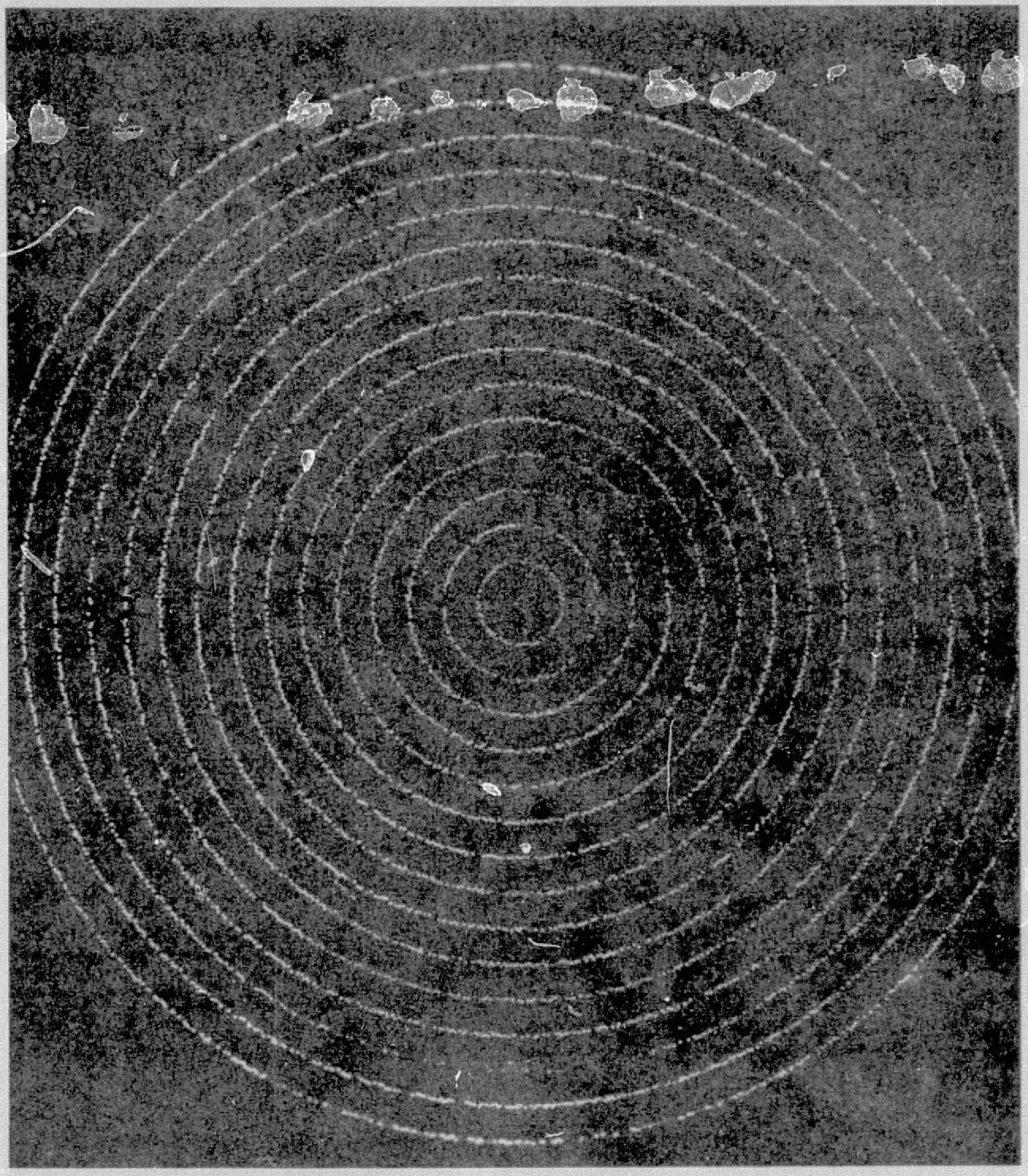

Figure 9B. Fiber Optic Array Light Distribution Resulting From Illumination of Column 11 on the Fiber Bundle Mounting Plate.

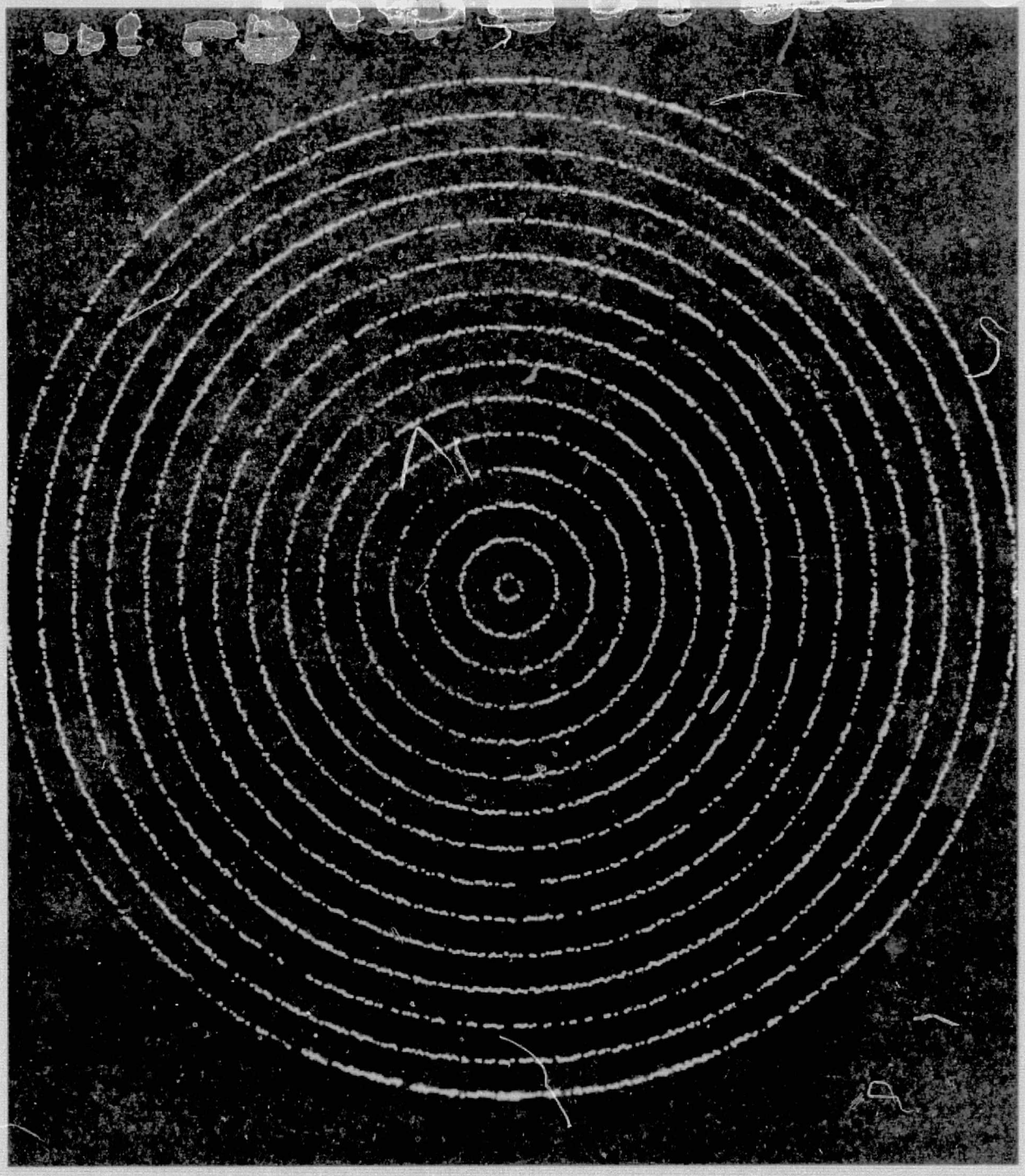

Figure 9C. Fiber Optic Array Light Distribution Resulting from Illumination of Column 1 on the Fiber Bundle Mounting Plate.

During this observation it was also discovered that some bundles contained one or more stray fibers belonging to another ring. These strays were traced and removed by illuminating one bundle at a time and locating the ring to which the stray belonged. None of the irregularities discovered during the testing phase caused undue concern since the fiber optic detector characteristic, once known, can be smoothed out during the digital processing operations.

## IV. OPTICAL/ELECTRONIC INTERFACE

The electronic portion of the Fourier transform detector provides the interface between the fiber optics array, consisting of a central fiber and bundles from 168 concentric rings, and a digital data processing system. The electronic system consists of (1) the photodiodes, (2) a current-to-voltage converter for each of the photodiodes, (3) an electronic commutating system, (4) a sample-and-hold circuit and an analog-to-digital converter. The digital processing system consists of a computer interface, a digital processor, and a data display system.

The photodiodes are mounted in a metal plate which is placed in contact with a similar plate in which the fiber optic bundles are terminated. The diodes are arranged in sixteen rows, the sixteenth row containing four diodes, and the remaining fifteen rows containing eleven diodes each. Figure 10 is a photograph of the photodiode mounting plate showing this layout. As described in Section III, three sizes of diodes are used. The central fiber and the first thirty rings are terminated with PIN-3DP photodiodes (United Detector Technology, Inc.). Rings numbered 31 through 121 are terminated in PIN-5DP photodiodes, and the remaining 46 rings are terminated in PIN-6DP photodiodes. A photograph of the arrangement of the photodiodes and the circuit boards is shown in Figure 10.

Each photodiode provides the input to a current-to-voltage converter. A converter consists of one-half of a μA747 operational amplifier. The converters have a conversion ratio of 1V/μAMP. One hundred and sixty-nine of the current-to-voltage converters are required--one for each photodiode. These converters are located on six printed circuit boards mounted just above the photodiodes.

The outputs of the current-to-voltage converters are connected to the inputs of six high level multiplexers (HP-12751A) in a Hewlett-Packard 2313B analog-to-digital interface subsystem. Each of the six high level multiplexers provides for 32 single ended inputs, giving a total input capability for the six boards of 192 channels. Only nine channels are used on the last board.

Figure 10. Arrangement of Photodiodes and Circuit Boards.

The sample-and-hold amplifiers and analog-to-digital converter are contained in the 2313B subsystem. The analog-to-digital converter is a 12 bit converter which gives 4096 quantization levels over an input voltage range of -10.24 to 10.235 volts in 5 millivolt steps.

The interface with a Hewlett-Packard 2100 series digital computer is provided by an interface board in the 2313B subsystem and an interface board in an input-output slot in the computer.

The 2100 series computer provides the means of reading the data from the 2313B subsystem, performing processing of the data to get it into the proper form for the various display capabilities, and outputing the data to either a teletype for hard copy recording or to an oscilliscope for real time display purposes.

## A. Subsystems Description

A block diagram of the electronic system is shown in Figure 11. The heart of the system is a Hewlett-Packard 2100 series computer which has input commands entered and responds in an interactive mode via a teletype terminal. The computer operates the 2313B subsystem which commutates the 169 analog input channels. It also outputs the processed data to an oscilloscope which provides a visual display of the spatial frequency data, or provides for printing of the data by means of a teletype-terminal.

The photodiodes are connected to the input channels of the 2313B subsystem by means of current-to-voltage converters. A schematic diagram of two of the 169 current-to-voltage converters is shown in Figure 12. Each of the converters make use of one-half of a μA747 operational amplifier.

The input voltage range of the analog-to-digital converter in the Hewlett-Packard 2313B subsystem is -10.24 to 10.235 volts. To make use of the full range of the converter, the zero light value must be offset to the most positive output voltage of the current-to-voltage converters. The cathode of the photodetector is grounded, and hence increasing light intensity drives the output of the current-to-voltage converters in a negative direction. Maximum light intensity is that which results in a negative input voltage to the analog-to-digital converter which is equal to -10.24V.

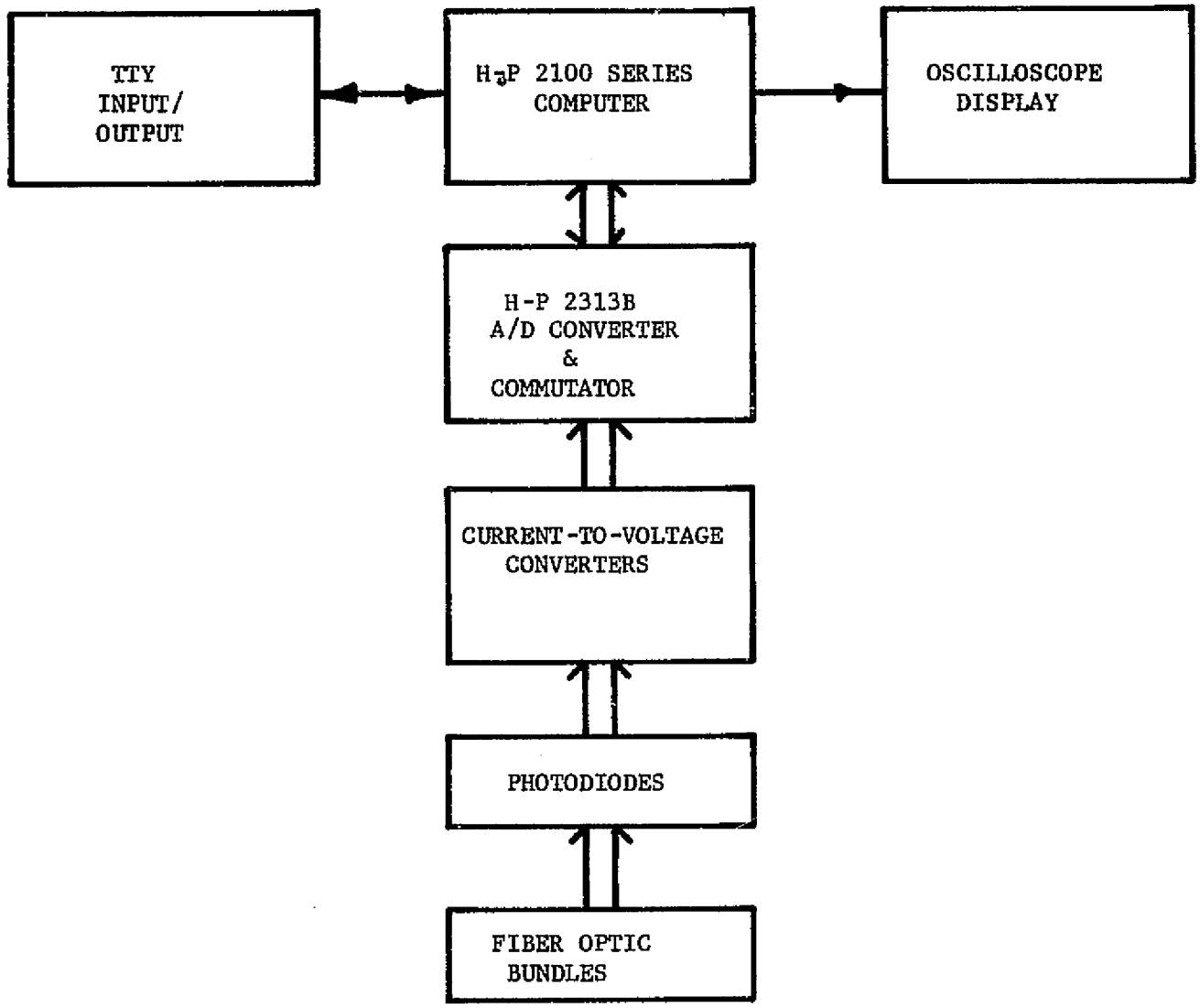


Figure 11. Block Diagram of Optical Processor Electronic System.

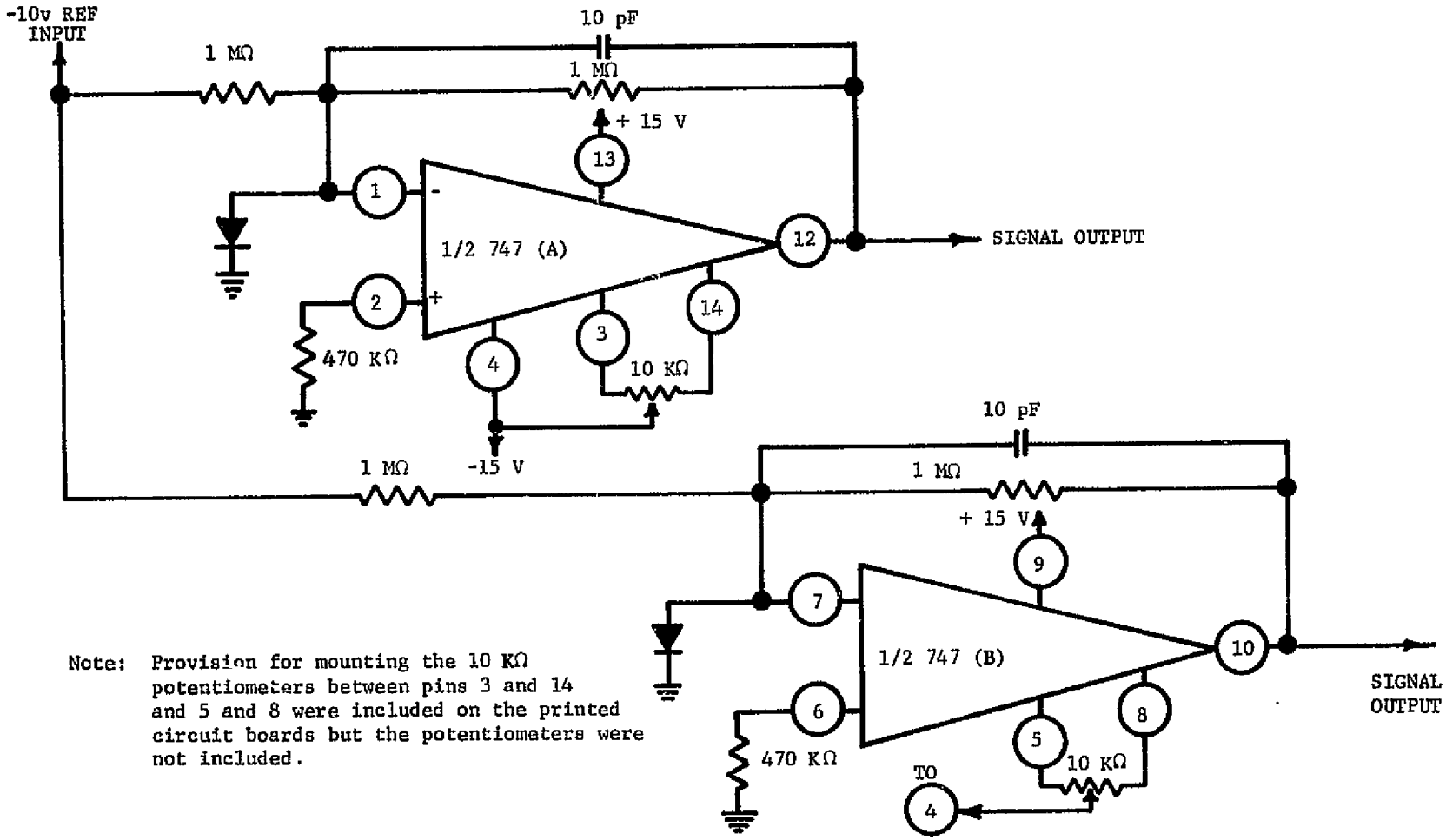


Figure 12. Schematic Diagram of a Dual Current-to-Voltage Converter.

To offset the output voltage of the current-to-voltage converters in this manner an input reference voltage is summed into the input of the converters as shown in Figure 12. The source of this stable reference voltage is shown in the schematic diagram of the reference voltage supply (Figure 13). The reference supply uses a temperature stabilized zener diode and an operational amplifier to supply the nominal -10 volt reference required. Only one reference supply is used and it is located on circuit board number one. All the other five circuit boards receive their reference supply from this source.

A photograph of one of the circuit boards is shown in Figure 14. To provide the interface between the rows of photodiodes, containing eleven diodes per row, and the input to the 2313B multiplexer cards, which have thirty-two single ended inputs per card, a single circuit board design requiring space for thirty-eight operational amplifiers (nineteen packages) was provided on each circuit board. Only those amplifiers needed for a specific board were mounted on the particular circuit board. Hence, each of the six circuit boards were made alike, but each has a different arrangement of components and a different jumper arrangement.

The photodiodes are connected to the circuit boards through a 56 and a 72 contact printed circuit connector for each circuit board, and the circuit board plugs into these connectors which are mounted end to end. On the top of each circuit board are the printed circuit contacts to mate with a 48 contact printed circuit connector which connects the current-to-voltage converter outputs to the inputs of the high level commutators in the 2313B subsystem. The cables which are used to interconnect the current-to-voltage converters and the 2313B contain 32 miniature coaxial cables and are wired so that each channel is connected in the same order in each connector. Each of the cables are wired alike.

Visible in the photograph of Figure 5 are the printed circuit contacts which mate with the 72 contact connector on the left and the 56 contact connector on the right. The reference supply is the circuit nearest the right edge of the board (present only on circuit board number one). The rest of the integrated circuit packages are the current-to-voltage

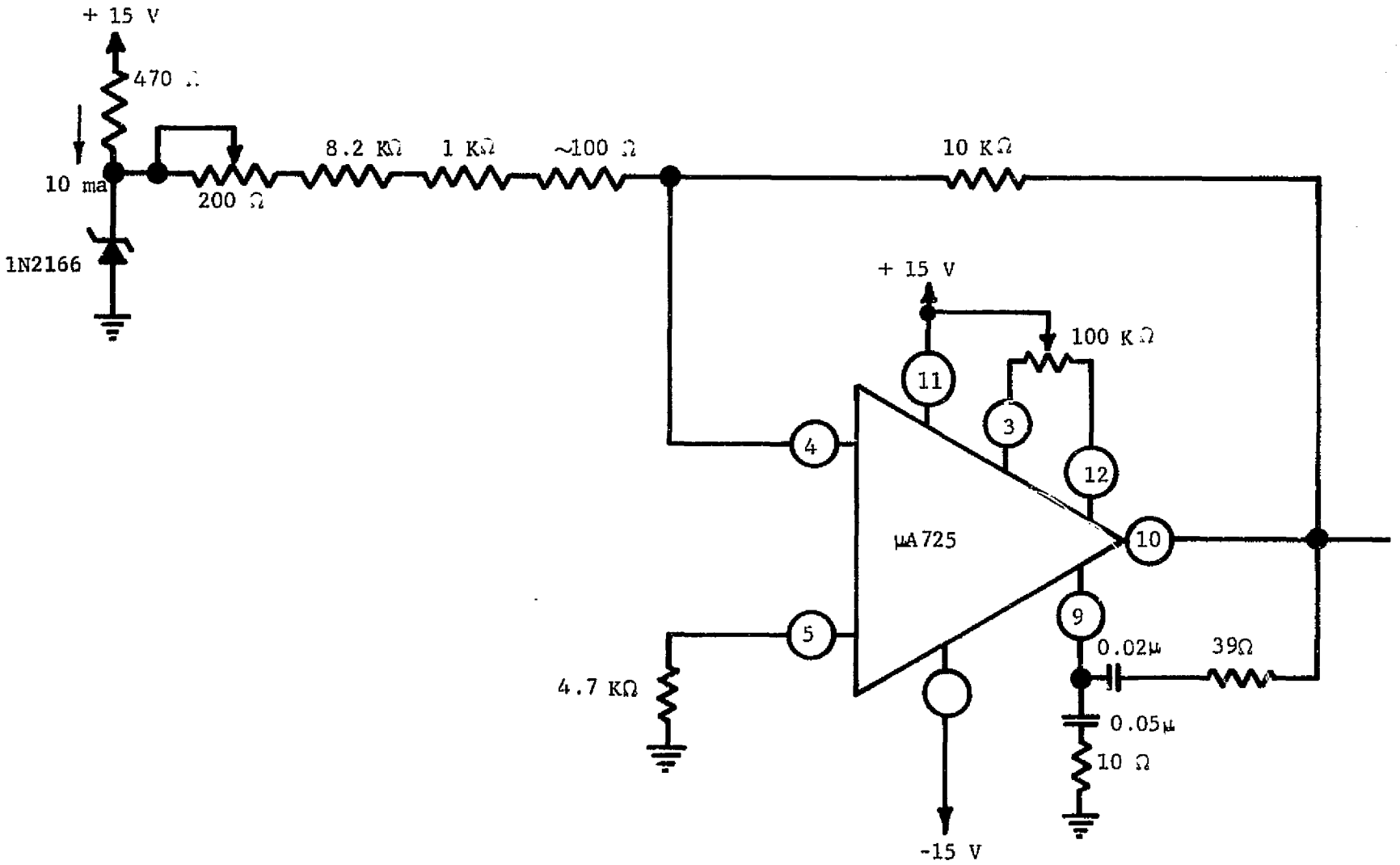


Figure 13. Schematic of Reference Voltage Supply.

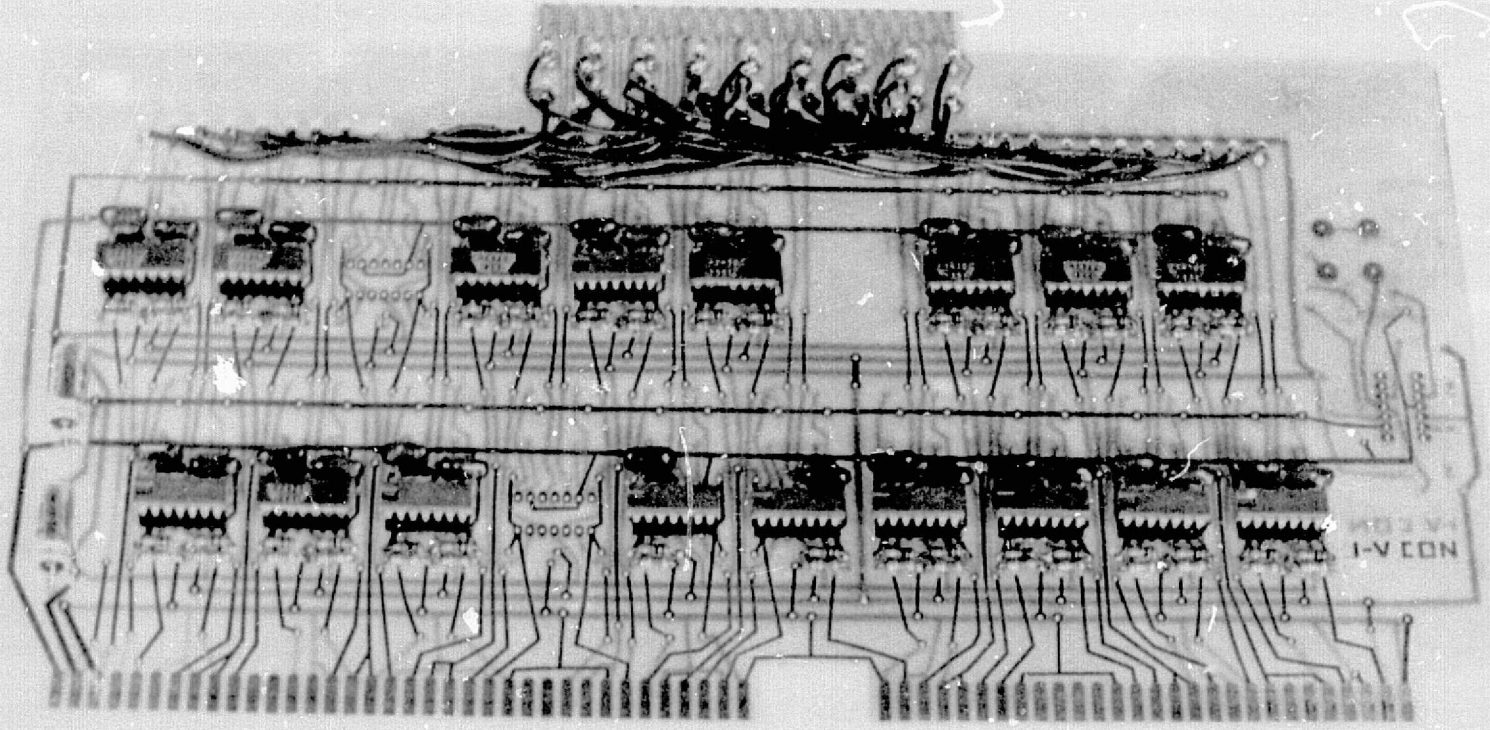


Figure 14. Photograph of a Typical Circuit Board (Circuit Board No. 2).

converters. Only those amplifier positions required to provide the necessary output for each of the six boards are connected on a specific board. There are positions for 38 individual amplifiers on each board, and the amplifiers are designated by a number from 1 to 38. The top row of amplifiers consists of nine integrated circuit packages containing 18 amplifiers. From left to right the amplifiers are designated by numbers A1-2, A5-6, A9-10, A13-14, A17-18, A21-22, A27-28, A31-32, and A35-36. Each of the integrated circuit packages contains two amplifiers. The bottom row, from left to right contains amplifiers A3-4, A7-8, A11-12, A15-16, A19-20, A23-24, A25-26, A29-30, A33-34 and A37-38. The outputs of each of the current-to-voltage converters which uses one of the amplifiers has its output connected to one of the pins in the row near the top edge of the circuit board running straight across the board. The amplifier output pins are numbered from 1 to 38 from left to right as shown in Figure 14. The printed circuit contacts at the top of the board are those which mate with the 38 contact connector which connects the current-to-voltage converters to the 2313B subsystem. Each of the 32 contacts at the top of the board, which are analog channel inputs, are terminated in pins just below the top printed circuit connector conductors. Jumpers are used to connect the appropriate amplifier output (from the row of 38 pins) to the appropriate pin for the output connector. Thirty-two amplifiers are connected on the first five boards. Only nine are connected on the sixth board.

Figure 15 shows the input and output connections to a circuit board. The input connections are shown for all possible diode input connections. Only a maximum of 32 input connections are used per board. The diode which collects light from the center fiber is connected to amplifier 29 on circuit board number one. This diode has its cathode connected to pin Y on the 56 pin connector and its anode connected to pin Z. Tables VI through XI indicate the input connector pin number to which the diodes anodes are connected, the amplifier used, and the output connector pin number to which the amplifier is jumpered for each of the six board. Figure 15 also gives the corresponding pins to which the diode cathodes are connected. For example, the center fiber, which is designated channel one, is connected to

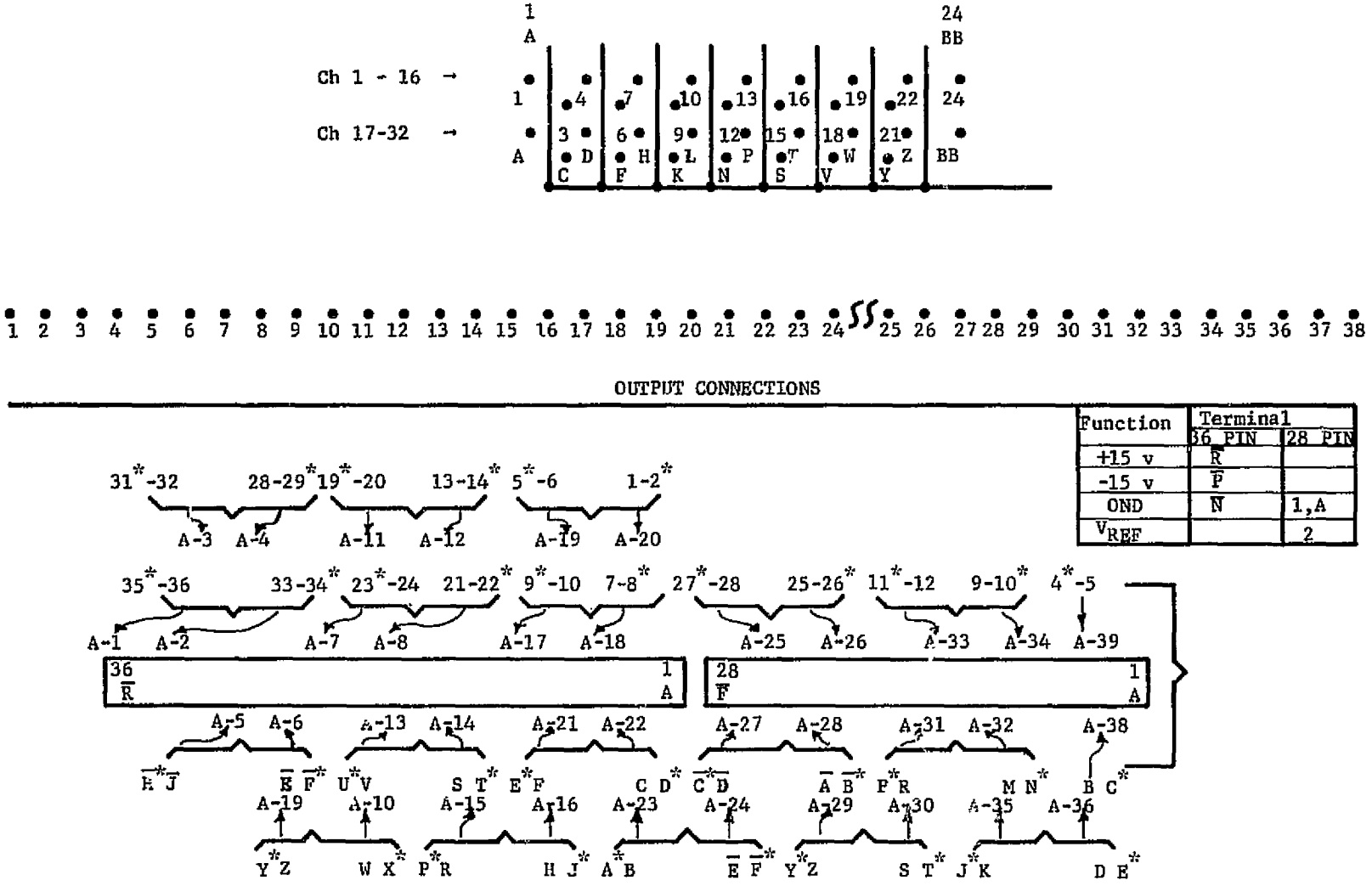


*Denotes Common or Ground Connection

Figure 15. Circuit Board Input and Output Connections.

TABLE VI

CIRCUIT BOARD NO. 1 CONNECTIONS

| 2313B HLMPX Card 1 (Slot 3) Channel No. | Input Connector and Contact to Which Diode Anode Is Connected | Amplifier | Output Connector Contact |
|---|---|---|---|
| 1 | 56-Z | A-29 | 1 |
| 2 | 56-S | A-30 | 3 |
| 3 | 56-K | A-35 | 4 |
| 4 | 56-D | A-36 | 6 |
| 5 | 72-$\overline{J}$ | A-5 | 7 |
| 6 | 72-$\overline{E}$ | A-6 | 9 |
| 7 | 72-V | A-13 | 10 |
| 8 | 72-S | A-14 | 12 |
| 9 | 72-F | A-21 | 13 |
| 10 | 72-C | A-22 | 15 |
| 11 | 56-$\overline{D}$ | A-26 | 16 |
| 12 | 56-$\overline{A}$ | A-28 | 18 |
| 13 | 56-R | A-31 | 19 |
| 14 | 56-M | A-32 | 21 |
| 15 | 56-B | A-38 | 22 |
| 16 | 72-36 | A-1 | 24 |
| 17 | 72-33 | A-2 | A |
| 18 | 72-24 | A-7 | C |
| 19 | 72-71 | A-8 | D |
| 20 | 72-10 | A-17 | F |
| 21 | 72-7 | A-18 | H |
| 22 | 56-28 | A-25 | K |
| 23 | 56-25 | A-26 | L |
| 24 | 56-12 | A-33 | N |
| 25 | 56-9 | A-34 | P |
| 26 | 56-5 | A-37 | S |
| 27 | 72-32 | A-3 | T |
| 28 | 72-28 | A-4 | V |
| 29 | 72-20 | A-11 | W |
| 30 | 72-13 | A-12 | Y |
| 31 | 72-6 | A-19 | Z |
| 32 | 72-1 | A-20 | BB |

TABLE VII

CIRCUIT BOARD NO. 2 CONNECTIONS

| 2313 HLMPX Card 2 (Slot 4) Channel No. | Input Connector and Contact to Which Diode Anode Is Connected | Amplifier | Output Connector Contact |
|---|---|---|---|
| 33 | 56-$\overline{E}$ | A-24 | 1 |
| 34 | 56-Z | A-29 | 3 |
| 35 | 56-S | A-30 | 4 |
| 36 | 56-K | A-35 | 6 |
| 37 | 56-D | A-36 | 7 |
| 38 | 72-$\overline{J}$ | A-5 | 9 |
| 39 | 72-$\overline{E}$ | A-6 | 10 |
| 40 | 72-V | A-13 | 12 |
| 41 | 72-S | A-14 | 13 |
| 42 | 72-F | A-21 | 15 |
| 43 | 72-C | A-22 | 16 |
| 44 | 56-$\overline{D}$ | A-27 | 18 |
| 45 | 56-$\overline{A}$ | A-28 | 19 |
| 46 | 56-R | A-31 | 21 |
| 47 | 56-M | A-32 | 22 |
| 48 | 56-B | A-38 | 24 |
| 49 | 72-36 | A-1 | A |
| 50 | 72-33 | A-2 | C |
| 51 | 72-24 | A-7 | D |
| 52 | 72-21 | A-8 | F |
| 53 | 72-10 | A-17 | H |
| 54 | 72-7 | A-18 | K |
| 55 | 56-28 | A-25 | L |
| 56 | 56-25 | A-26 | N |
| 57 | 56-12 | A-33 | P |
| 58 | 56-9 | A-34 | S |
| 59 | 56-5 | A-37 | T |
| 60 | 72-32 | A-3 | V |
| 61 | 72-28 | A-4 | W |
| 62 | 72-20 | A-11 | Y |
| 63 | 72-13 | A-12 | Z |
| 64 | 72-6 | A-19 | BB |

TABLE VIII

CIRCUIT BOARD NO. 3 CONNECTIONS

| HP2313 HLMPX Card 3 (Slot 5) Channel No. | Input Connector and Contact to Which Diode Anode Is Connected | Amplifier | Output Connector Contact |
|---|---|---|---|
| 65 | 72-B | A-23 | 1 |
| 66 | 56-$\overline{E}$ | A-24 | 3 |
| 67 | 56-Z | A-29 | 4 |
| 68 | 56-S | A-30 | 6 |
| 69 | 56-K | A-35 | 7 |
| 70 | 56-D | A-36 | 9 |
| 71 | 72-$\overline{J}$ | A-5 | 10 |
| 72 | 72-$\overline{E}$ | A-6 | 12 |
| 73 | 72-V | A-13 | 13 |
| 74 | 72-S | A-14 | 15 |
| 75 | 72-F | A-21 | 16 |
| 76 | 72-C | A-22 | 18 |
| 77 | 56-$\overline{D}$ | A-27 | 19 |
| 78 | 56-$\overline{A}$ | A-28 | 21 |
| 79 | 56-R | A-31 | 22 |
| 80 | 56-M | A-32 | 24 |
| 81 | 56-B | A-38 | A |
| 82 | 72-36 | A-1 | C |
| 83 | 72-33 | A-2 | D |
| 84 | 72-29 | A-7 | F |
| 85 | 72-21 | A-8 | H |
| 86 | 72-10 | A-17 | K |
| 87 | 72-7 | A-18 | L |
| 88 | 56-28 | A-25 | N |
| 89 | 56-25 | A-26 | P |
| 90 | 56-12 | A-33 | S |
| 91 | 56-9 | A-34 | T |
| 92 | 56-5 | A-37 | V |
| 93 | 72-32 | A-3 | W |
| 94 | 72-28 | A-4 | Y |
| 95 | 72-20 | A-11 | Z |
| 96 | 72-13 | A-12 | BB |

TABLE IX

CIRCUIT BOARD NO. 4 CONNECTIONS

| 2313 HLMPX Card 4 (Slot 6) Channel No. | Input Connector and Contact to Which Diode Anode Is Connected | Amplifier | Output Connector Contact |
|---|---|---|---|
| 97 | 72-H | A-16 | 1 |
| 98 | 72-$\overline{B}$ | A-23 | 3 |
| 99 | 56-$\overline{E}$ | A-24 | 4 |
| 100 | 56-Z | A-29 | 6 |
| 101 | 56-S | A-30 | 7 |
| 102 | 56-K | A-35 | 9 |
| 103 | 56-$\overline{D}$ | A-36 | 10 |
| 104 | 72-$\overline{J}$ | A-5 | 12 |
| 105 | 72-$\overline{E}$ | A-6 | 13 |
| 106 | 72-V | A-13 | 15 |
| 107 | 72-S | A-14 | 16 |
| 108 | 72-F | A-21 | 18 |
| 109 | 72-C | A-22 | 19 |
| 110 | 56-$\overline{D}$ | A-27 | 21 |
| 111 | 56-$\overline{A}$ | A-28 | 22 |
| 112 | 56-R | A-31 | 24 |
| 113 | 56-M | A-32 | A |
| 114 | 56-B | A-38 | C |
| 115 | 72-36 | A-1 | D |
| 116 | 72-33 | A-2 | F |
| 117 | 72-24 | A-7 | H |
| 118 | 72-21 | A-8 | K |
| 119 | 72-10 | A-17 | L |
| 120 | 72-7 | A-18 | N |
| 121 | 56-28 | A-25 | P |
| 122 | 56-25 | A-26 | S |
| 123 | 56-12 | A-33 | T |
| 124 | 56-9 | A-34 | V |
| 125 | 56-5 | A-37 | W |
| 126 | 72-32 | A-3 | Y |
| 127 | 72-28 | A-4 | Z |
| 128 | 72-20 | A-11 | BB |

TABLE X

CIRCUIT BOARD NO. 5 CONNECTIONS

| 2313B HLMPX Card 5 (Slot 7) Channel No. | Input Connector and Contact to Which Diode Anode Is Connected | Amplifier | Output Connector Contact |
|---|---|---|---|
| 129 | 72-R | A-15 | 1 |
| 130 | 72-H | A-16 | 3 |
| 131 | 72-B | A-23 | 4 |
| 132 | 56-$\overline{E}$ | A-24 | 6 |
| 133 | 56-Z | A-29 | 7 |
| 134 | 56-S | A-30 | 9 |
| 135 | 56-K | A-35 | 10 |
| 136 | 56-D | A-36 | 12 |
| 137 | 72-$\overline{J}$ | A-5 | 13 |
| 138 | 72-$\overline{E}$ | A-6 | 15 |
| 139 | 72-V | A-13 | 16 |
| 140 | 72-S | A-14 | 18 |
| 141 | 72-F | A-21 | 19 |
| 142 | 72-C | A-22 | 21 |
| 143 | 56-$\overline{D}$ | A-27 | 22 |
| 144 | 56-$\overline{A}$ | A-28 | 24 |
| 145 | 56-R | A-31 | A |
| 146 | 56-M | A-32 | C |
| 147 | 56-B | A-38 | D |
| 148 | 72-36 | A-1 | F |
| 149 | 72-33 | A-2 | H |
| 150 | 72-24 | A-7 | K |
| 151 | 72-21 | A-8 | L |
| 152 | 72-10 | A-17 | N |
| 153 | 72-7 | A-18 | P |
| 154 | 56-28 | A-25 | S |
| 155 | 56-25 | A-26 | T |
| 156 | 56-12 | A-33 | V |
| 157 | 56-9 | A-34 | W |
| 158 | 56-5 | A-37 | Y |
| 159 | 72-32 | A-3 | Z |
| 160 | 72-38 | A-4 | BB |

TABLE XI

CIRCUIT BOARD NO. 6 CONNECTIONS

| 2313B HLMPX Card 6 (Slot 8) Channel No. | Input Connector and Contact to Which Diode Anode Is Connected | Amplifier | Output Connector Contact |
|---|---|---|---|
| 161 | 72-W | A-10 | 1 |
| 162 | 72-R | A-15 | 3 |
| 163 | 72-H | A-16 | 4 |
| 164 | 72-B | A-23 | 6 |
| 165 | 56-$\overline{E}$ | A-24 | 7 |
| 166 | 56-Z | A-29 | 9 |
| 167 | 56-S | A-30 | 10 |
| 168 | 56-K | A-35 | 12 |
| 169 | 56-D | A-36 | 13 |

The remaining 23 input channels are unused.

pin Z on the 56 contact connector, and uses amplifier number 29, which is connected to output connector contact number one. The diodes are numbered from left to right looking down from the circuit board locations (see Figure 10). The bottom row contains diodes 1 through 4, the second row up contains diodes 5 through 15, etc. The first diode on the second board represents commutator channel number 33, is connected to pin E on the 56 pin connector, uses amplifer 24, and is jumpered to output connector pin 1 (see Table VII). The last diode used (channel 169) has its anode connected to pin D on the 56 pin connector, uses amplifier 36 whose output is jumpered to output connector pin 13 (see Table XI). Using the connection techniques allows one circuit board design to be used for each of the six circuit boards.

The circuit boards were laid out with the provision of mounting offset null potentiometers to zero the output voltage of the operational amplifiers. These were not mounted and the techniques for handling the variation in zero light level output voltage will be discussed in connection with the computer programs.

Power for the current-to-voltage converters is supplied from a Lambda Model LCD-4-22 power supply which furnishes $\pm$ 15 volts for the operational amplifiers and reference voltage supply. This power supply is mounted in a separate 19 inch rack panel and is connected to the current-to-voltage converters by means of the small Winchester connector on the box housing the converters.

## B. Computer Program

The computer program used to operate the 2313B subsystem and to generate various forms of output data is described in this section. The output data may be hard copy generated on a teletype terminal or it may be a real time display of the spatial frequency data on an oscilloscope. The HP 2100 Series computer switch register is used to control the output modes. The program uses a main program written in FORTRAN and five subroutines--two in FORTRAN and three in Assembly language.

The main program, shown in Figure 16, controls the reading and display of the data. The first response of the program after it is started is the statement "Enter N". N is the number of sequential 2313B commutator channels which are to be sampled starting from the first channel which receives light from the center fiber. N can have any value from 1 to 169 which allows for reading of the data from the central fiber or the central fiber and the selected number of rings up to 168. Storage is not allocated for reading from more than 169 channels although 192 are available with the six high level multiplexer cards.

Reading and scaling of the data from the 2313B subsystem is performed by the FORTRAN subroutine RDAD shown in Figure 17. This subroutine calls the assembly language subroutine RD (Figure 18) to actually read the 2313B subsystem. Adding subroutine RD was a last minute change to accommodate the DOS-III system on the 2116B computer. The original RDAD subroutine used the HP BCS and the HP Fortran driver I2313 for the 2313B subsystem. The original RDAD subroutine is shown in Figure 19. Its operation will be described. The first call to the driver normalizes A/D conversion system, the second makes the readings, and the third checks the status to see if the readings have been completed. The data is read into the integer array IBF, the twelve bit data word occupying the 12 most significant bits of the computer word. This same function is performed in the DOS-III system by the subroutine RD. Conversion of the integer array to real numbers and scaling is also accomplished in this subroutine. The scaling accounts for the bit positions in the word converting the integer word values to floating point. The floating point data in the real array DATA has the range of zero to +20.475 volts. Channels for which data was not read contain the value zero.

The first call to the subroutine RDAD by the main program is for the purpose of reading zero light intensity values. These readings should be made with illumination removed from the input to the fiber optic bundles to compensate for ambient background light or any other light distribution which must be eliminated from the diffraction pattern. The readings vary from channel to channel partly because the balance pots to zero the

```
0001          FTN
0002          PROGRAM MAIN
0003          DIMENSION ZIDTA(169)
0004          COMMON N,IBF(169),DATA(169),ALDTA(169)
0005          CALL EXEC(30,1)
0006          WRITE(1,200)
0007          READ(1,*) N
0008          CALL RDAD
0009          DO 5 I=1,169
0010        5 ZIDTA(I) = DATA(I)
0011          IF (IS(0)) 10,20,10
0012       10 WRITE(1,201)
0013          READ(1,*) NR1,NP1
0014          DO 15 I = NR1,NP1
0015       15 WRITE(1,211) I,DATA(I)
0016       20 CALL RDAD
0017          IF (IS(1)) 30,40,30
0018       30 WRITE(1,202)
0019          READ(1,*) NR1,NP1
0020          DO 35 I = NR1,NP1
0021       35 WRITE(1,211) I,DATA(I)
0022       40 DO 44 I = 1,N
0023       44 DATA(I) = DATA(I) - ZIDTA(I)
0024          IF (IS(2)) 50,60,50
0025       50 WRITE(1,203)
0026          READ(1,*) NR1,NP1
0027          DO 55 I = NR1,NP1
0028       55 WRITE(1,211) I,DATA(I)
0029       60 CALL LGDTA
0030          IF (IS(4)) 70,80,70
0031       70 WRITE(1,204)
0032          READ(1,*) NR1,NP1
0033          DO 75 I = NR1,NP1
0034          TEMP = (ALDTA(I)/128. - 255.) / 6.375
0035       75 WRITE(1,217)I,TEMP
0036       80 CALL WTDAL
0037          GO TO 20
0038      200 FORMAT("ENTER N")
0039      201 FORMAT("ENTER NSTART, NSTOP FOR ZERO INT DATA")
0040      202 FORMAT("ENTER NSTART, NSTOP FOR UNCOR DATA")
0041      203 FORMAT("ENTER NSTART, NSTOP FOR COR DATA")
0042      204 FORMAT("ENTER NSTART, NSTOP FOR LOG DATA")
0043      211 FORMAT(1X,I3,1X,F9.4)
0044      217 FORMAT(1X,I3,3X,F7.2)
0045          END
0046          END$
**** LIST END ****
```

Figure 16. Main Fortran Program.

```
0001          FTN
0002          SUBROUTINE RDAD
0003          COMMON N,IBF(169),DATA(169),ALDTA(169)
0004          CALL RD
0005          NN = N + 1
0006          DO 8 I = NN,169
0007          IBF(I) = 100000B
0008        8 DATA(I) = 0.
0009          DO 7 I = 1,N
0010        7 DATA(I) = -(FLOAT(IAND(IBF(I),177760B)) * .0003125 - 1
0011          RETURN
0012          END
0013          END$
**** LIST END ****
```

Figure 17. Subroutine RDAD for Reading and Scaling Data from the HP 2313B Subsystem.

```
0001   ASMB,R,B,L,T
0002           NAM RD,7
0003           ENT RD
0004           COM N,IBF(169)
0005   CLC     OCT 106725
0006           LDA CLC
0007           STA 25B
0008   RD      NOP
0009           LDA RD,I
0010           STA RTRN
0011           LDA N
0012           CMA,INA
0013           STA CTR
0014           LDA MPXR
0015           STA CODE
0016           LDA ILOC
0017           STA LOC
0018           LDB CTR
0019           CLC 25B
0020   LOOP    LDA CODE
0021           OTA 25B
0022           STC 25B,C
0023           SFS 25B
0024           JMP *-1
0025           LIA 25B
0026           SFS 25B
0027           JMP *-1
0028           STA LOC,I
0029           ISZ CODE
0030           ISZ LOC
0031           INB,SZB
0032           JMP LOOP
0033           JMP RTRN,I
0034   RTRN    BSS 1
0035   CTR     BSS 1
0036   MPXR    OCT 100140
0037   CODE    BSS 1
0038   ILOC    DEF IBF
0039   LOC     BSS 1
0040           END
**** LIST END ****
```

Figure 18. Subroutine RD.

```
      SUBROUTINE RDAD
      COMMON N,IBF(169),DATA(169),ALDTA(169)
      CALL I2313(7,0)
      CALL I2313(7,2,0,2,000140B,N,IBF,0)
    5 CALL I2313(7,1,ISTAT,ITLOG)
      IF(ISTAT) 5,6
    6 CONTINUE
      NN = N + 1
      DO 8 I = NN,169
      IBF(I) = 100000B
    8 DATA(I) = 0.
      DO 7 I = 1,N
    7 DATA(I) = -(FLOAT(IAND(IBF(I),177760B)) * .0003125 - 10.235)
      RETURN
      END
      ENDS
```

Figure 19. Original RDAD Subroutine.

operational amplifier output were not included on the circuit boards. If it is desirable to print these zero intensity values switch register bit zero should be set equal to one. This bit is effective only when the program is stated, other active switch register bits may be activated at any time. If switch register bit zero is set to one, the program responds with "Enter N start, N stop for Zero Int Data". This allows any portion of the zero intensity readings to be printed on the teletype. If switch register bit zero is zero when the program is stated, the program proceeds to act on the status of switch register bits one through four.

The function of the switch register bits one through four control the printing of data in various forms and the oscilloscope display of data. Bit one on allows for the printing of uncorrected data, that is, data from which the zero intensity values have not been subtracted. Bit two on provides for the printing of corrected data. Corrected data is that data for which the zero light intensity values have been subtracted from the actual readings. Bit three on provides for real time display of the logarithm of the corrected data on an oscilloscope display. The display is operated in a refreshed mode so that changes in the measured data may be observed as changed in the spatial data are made. Switching bit three off causes a continuous display of the data that was in storage when bit three was switched off or when the program entered the WTDAL subroutine.

Switch register bit four controls the printing of the logarithm of the input data. Bit four on generates a request for the number of the channel where print of the data is to begin and where it is to stop.

Use of the switch register as described is accomplished through the assembly language coded function IS shown in Figure 20. It interrogates the status of the switch register (S-register) bit n in the 2100 series computer and returns a zero if the bit is off and to a non-zero value otherwise. The function is used to switch to two different sets of instructions depending on the status of bit n in the switch register. Switching is accomplished by arithmetic IF statements in the main program. Since the switch register is active during the time that the computer is running, use of the function IS provides a means of implementing optional features that can be accessed during the coarse of a run.

```
0001  ASMB,R,B,L,T
0002         NAM IS,7
0003         ENT IS
0004         EXT .ENTR
0005  CLC    106701
0006  AGMT   BSS 1
0007  IS     NOP
0008         JSB .ENTR
0009         DEF AGMT
0010         LDA CLC
0011         STA 1B
0012         LDA AGMT,I
0013         SSA
0014         JMP IS,I
0015         CMA
0016         CLB,CCE
0017         ELB,CLE
0018         INA,SZA
0019         JMP *-2
0020         LIA 1
0021         AND 1
0022         JMP IS,I
0023         END
**** LIST END ****
```

Figure 20. Assembly Language Routine IS.

Output of the data to the oscilloscope for display purposes is provided with the amplitude having logarithmetic values. This allows observation of light levels over a dynamic range greater than three orders of magnitude. The logarithm of the data is computed in the FORTRAN subroutine LGDA shown in Figure 21. The data in array DATA is placed in array ALDTA in normalized form. The data is tested for zero or negative values before the logarithm is taken, and for any data having these values the value of -40 dB is inserted in its place in the array ALDTA. The logarithm of valid data is inserted in its proper place in the array ALDTA.

The last operation in the subroutine LGDTA is the scaling of the data for an 8 bit D/A converter (HP-12555B).

The assembly language subroutine WTDAL (Figure 22) is used to write the logarithm of the measured values on an oscilloscope. This subroutine places a dot on the oscilloscope display at 10 dB intervals in the vertical direction along the same vertical line where channel one data is displayed. The horizontal axis is marked with dots every ten channels for 200 channels at the -40 dB level.

## C. Subsystem Characteristics

When the system is initially set up, the reference voltage from the reference voltage supply on circuit board number one must be set so that all of the zero light intensity output voltages of the current-to-voltage converters are within the input voltage range of the HP2313 analog to digital converter. To do this the computer program may be used to print the zero light intensity values. The input plane of the fiber optics bundles should be blocked to prevent ambient light from producing erroneous readings. The zero intensity values may be printed by setting switch register bit zero on before the program is started. All 169 channels should be printed. The voltage reading should be in the range of approximately one volt or less. If any channels read zero, this is an indication that the reference voltage is not set correctly. In tests conducted on the equipment, it was found that the reference voltage needed to be set to 9.736 volts to bring all channels on scale. The reference voltage may be measured at pin number 2 on the 56 pin connector with a digital

```
0001          FTN
0002          SUBROUTINE LGDTA
0003          COMMON N,IBF(169),DATA(169),ALDTA(169)
0004          DO 1 I = 1,169
0005          IF(DATA(I)) 2,2,3
0006        3 ALDTA(I) = DATA(I) / 20.475
0007          ALDTA(I) = 4.343 * ALOG(ALDTA(I))
0008          GO TO 1
0009        2 ALDTA(I) = -40.
0010        1 CONTINUE
0011          DO 20 I = 1,169
0012       20 ALDTA(I) = (255. + 6.375 * ALDTA(I)) * 128.
0013          RETURN
0014          END
0015          END$
**** LIST END ****
```

Figure 21. Fortran Subroutine LGDTA.

```
0001  ASMB,R,B,L,T
0002          NAM WTDAL,7
0003          ENT WTDAL
0004  IBLC    DEF ALDTA
0005          COM N,IBF(169),DATA(338),ALDTA(338)
0006  CLC     OCT 106716
0007  WTDAL   NOP
0008          LDA CLC
0009          STA 16B
0010          LDA WTDAL,I
0011          STA RETRN
0012  START   LDB ISTRT
0013          STB INDEX
0014          LDB XST
0015          STB X
0016          LDB IBLC
0017          STB ALDST
0018          SFS SCOPE
0019          JMP *-1
0020          CLF SCOPE
0021          LDA SCAST
0022          STA POS
0023          LDA XCTRS
0024          STA CTR
0025  XSCA    LDA POS
0026          OTA SCOPE
0027          ADA TEN
0028          STA POS
0029          ISZ CTR
0030          JMP XSCA
0031          LDA SCAST
0032          STA POS
0033          LDA YCTRS
0034          STA CTR
0035  YSCA    LDA POS
0036          OTA SCOPE
0037          ADA SIXF
0038          STA POS
0039          ISZ CTR
0040          JMP YSCA
0041          LDA ZDB
0042          OTA SCOPE
```

Figure 22. Subroutine WTDAL for Writing the Logarithm of the Observed Light Values on an Oscilloscope.

```
0043  LOOP   DLD ALDST,I
0044         FIX
0045         RAL
0046         AND MASK
0047         ADA X
0048         OTA SCOPE
0049         ISZ X
0050         ISZ ALDST
0051         ISZ ALDST
0052         ISZ INDEX
0053         JMP LOOP
0054         LIA 1
0055         AND IBIT3
0056         SZA
0057         JMP RETRN,I
0058         JMP START
0059  XST    OCT 1
0060  MASK   OCT 177400
0061  ISTRT  DEC -169
0062  RETRN  BSS 1
0063  INDEX  BSS 2
0064  SCOPE  EQU 16B
0065  X      EQU INDEX+1
0066  SCAST  DEC 0
0067  POS    BSS 1
0070  XCTRS  DEC -21
0069  CTR    BSS 1
0070  YCTRS  DEC -4
0071  YSCAR  OCT 200
0072  ALDST  BSS 1
0073  ZDB    OCT 177400
0074  TEN    DEC 10
0075  SIXF   OCT 40000
0076  IBIT3  OCT 10
0077         END
**** LIST END ****
```

Figure 22. (Concluded)

voltimeter. It is adjusted with the potentiometer located on the right hand side of printed circuit board number one nearest the center of the board. Once all the voltage readings are brought on scale, any light incident on the photodiodes will provide an in range input voltage to the analog to digital converter. A typical print out of the first thirty two zero light intensity voltages is shown in Figure 23.

Using some of the Hewlett-Packard furnished diagnostic software, histograms of the voltage reading on selected channels may be made. Figure 24 shows a histogram for the first ten channels. The histograms were obtained for 30,000 consecutive readings on each channel. A quiet channel is indicated by a small number of different voltage levels encountered during the time that the measurements were being taken. The entries for BX, CD, CH indicate the box number in the HP2313B subsystem for which the readings were taken (zero since this is the first 2313B box used), the printed circuit card in box zero (which is three for the first high level multiplexer card), and the channel number on the specified card. The channel numbers on a card are numbered from 0 to 31. Thus, Figure 24 shows the histograms for the first ten of the 169 used channels. Most of the channels show fairly quiet operation particularly channels numbered 3 and 8 for which all of the 30,000 readings occurred at a single value of voltage. Channel number one was the noisiest with six analog-to-digital converter steps excited during the 30,000 readings. While most of the readings occurred at 10.195 volts, a small number of values were scattered over adjacent converter steps.

```
ENTER N
169
ENTER NSTART, NSTOP FOR ZERO INT DATA
1,169
   1      .7650
   2      .3150
   3      .4400
   4      .2250
   5      .5650
   6      .5450
   7      .5500
   8      .5000
   9      .1650
  10      .5900
  11      .1700
  12      .4900
  13      .6750
  14      .7250
  15      .6600
  16      .1500
  17      .3250
  18      .9600
  19      .2300
  20      .5250
  21      .5300
  22      .5100
  23      .3000
  24      .2600
  25      .3800
  26      .4300
  27      .4100
  28      .2100
  29      .3300
  30      .9400
  31      .6250
  32      .4400
```

Figure 23. Zero Light Intensity Voltages for Channels 1-33.

```
>HI
 NO= 3000
 BX,CD,CH = 0 3 0
 AVG= 9.731192 PP=      .005001 HI=    9.735001  LO=    9.730000  RMS= .00213078
   9.730000          22850
   9.735001           7150

>HI
 NO= 3000
 BX,CD,CH = 0 3 1
 AVG= 10.195089 PP=     .025000 HI=  10.209999 LO=    10.184999 RMS= .00083666
  10.184999             4
  10.190000           100
  10.195000         29287
  10.199999           569
  10.205000            39
  10.209999             1

>HI
 NO= 30000
 BX,CD,CH = 0 3 2
 AVG= 10.054985 PP=     .010000 HI=  10.059999 LO=    10.049999 RMS= .00027952
  10.049999            93
  10.055000         29906
  10.059999             1

>HI
 NO= 30000
 BX,CD,CH = 0 3 3
 AVG= 10.235001 PP=     .000000 HI= 10.235001 LO=     10.235001 RMS= .00000000
  10.235001         30000

>HI
 NO= 30000
 BX,CD,CH = 0 3 4
 AVG= 9.933872 PP=      .004999 HI=   9.934999 LO=     9.930000 RMS= .00208931
   9.930000          6766
   9.934999         23234

>HI
 NO= 30000
 BX,CD,CH = 0 3 5
 AVG= 9.950611 PP=      .010000 HI=   9.955000 LO=     9.945000 RMS= .00163883
   9.945000             1
   9.949999         26330
   9.55000           3669

>HI
 NO= 30000
 BX,CD,CH = 0 3 6
 AVG= 9.947968 PP=      .004999 HI=   9.949999 LO=     9.945000 RMS=  .00245549
   9.945000         12195
   9.949999         17805

>HI
 NO= 30000
 BX,CD,CH = 0 3 7
 AVG= 10.004999 PP=     .005001 HI=  10.010000 LO=    10.004999 RMS= .00004083
  10.004999         29998
  10.010000             2

>HI
 NO= 30000
 BX,CD,CH = 0 3 8
 AVG= 10,235001 PP=     .000000 HI=  10.235001 LO=    10.235001 RMS= .00000000
  10.235001         30000

>HI
 NO= 30000
 BX,CD,CH = 0 3 9
 AVG= 9.909349 PP=      .004999 HI=   9.910000 LO=     9.905001 RMS= .00168362
   9.905001          3913
   9.910000         25087
```

Figure 24. Histograms of Voltage Readings on Selected Channels.

ORIGINAL PAGE IS
OF POOR QUALITY

## V. SYSTEM PERFORMANCE

The final measure of performance for a coherent optical processor for the subject application should be described in terms of the degree of success for which the desired pattern recognition operations can be performed. The goal of this program has been the development of an automatic diffraction pattern sampling system for classification of forested land areas from aerial photographs. The complexity of the system concept and the limited resources available have resulted in the major program emphasis being directed toward hardware development. In view of the hardware emphasis necessitated by the scope of this program, very little effort was expended in developing digital processing algorithms for classification of forestry images. Consequently, the preliminary performance criteria have been based on diffraction pattern sampling effectiveness.

The performance of the diffraction pattern sampling system consisting of the fiber optic detector and its associated electronic interface subsystem can be discussed in terms of its radial distribution function for uniform illumination, radiometric sensitivity, dynamic range for linear response, and adjacent ring cross coupling. As discussed in Section II, the concentric ring fiber optic detector divides the Fourier transform plane into zones of constant spatial frequency with finite bandwidth. The spatial frequency, $\nu_s$, is given by

$$\nu_s = \frac{dn}{\lambda f}, \tag{3}$$

where d is the diameter of the optical fiber,

n is the ring number,

$\lambda$ is the wavelength of the coherent optical source, and

f is the focal length of the Fourier transform lens.

The spatial frequency bandwidth, $\Delta\nu_s$, is constant for each zone, and is given by

$$\Delta\nu_s = \frac{d}{\lambda f} \tag{4}$$

The spatial frequency can be thought of as a scale factor relating periodic changes of object transparency to periodic changes in the intensity of the Fourier transform diffraction pattern. Since the object function can be approximated by a finite sum of properly weighted periodic grating functions, the analysis of the Fourier transform of any object can be approached in a systematic manner. It is, therefore, important to know how the diffraction plane detector weights the diffraction pattern as a function of spatial frequency.

The linearity of the photodetector-operational amplifier pairs was investigated by illuminating the photodetector with sufficient irradiance to produce the maximum 20 volt input of the HP 2313B subsystem, which was described in Section IV, and recording the voltage output as a function of decreasing irradiance. A typical linearity curve measured for a UDT - 5DP photodetector - μA 747 operational amplifier pair is shown in Figure 25. The linearity is shown to exceed the 36 dB dynamic range of the A/D converter.

The radial distribution function and the calculation of system sensitivity was based on the recording of the light background corrected output voltages of the 169 channels for illumination of the detector face by a uniform light source. It was found that this recording contained discontinuities in the distribution of points at the ring locations corresponding to changes in the photodiode types. An analysis of the photodiode - fiber optic bundle mounting geometry revealed that radiation losses were occurring because the active element of the photodiode, which is recessed about 0.3 cm below the window of the photodiode housing, subtends a much smaller solid angle than the radiation solid angle of the fiber optic bundle. Calculations were made to determine the losses incurred for each range of fiber bundles assigned to the three diode types. These calculations along with a diagram of the fiber bundle - photodiode mounting geometry is shown in Figure 26. When these loss components are included in the radial distribution characteristic of equation (1), the discontinuous behavior is accounted for.

The measured and calculated distribution characteristics for the complete diffraction pattern sampling system are shown in Figure 27. The

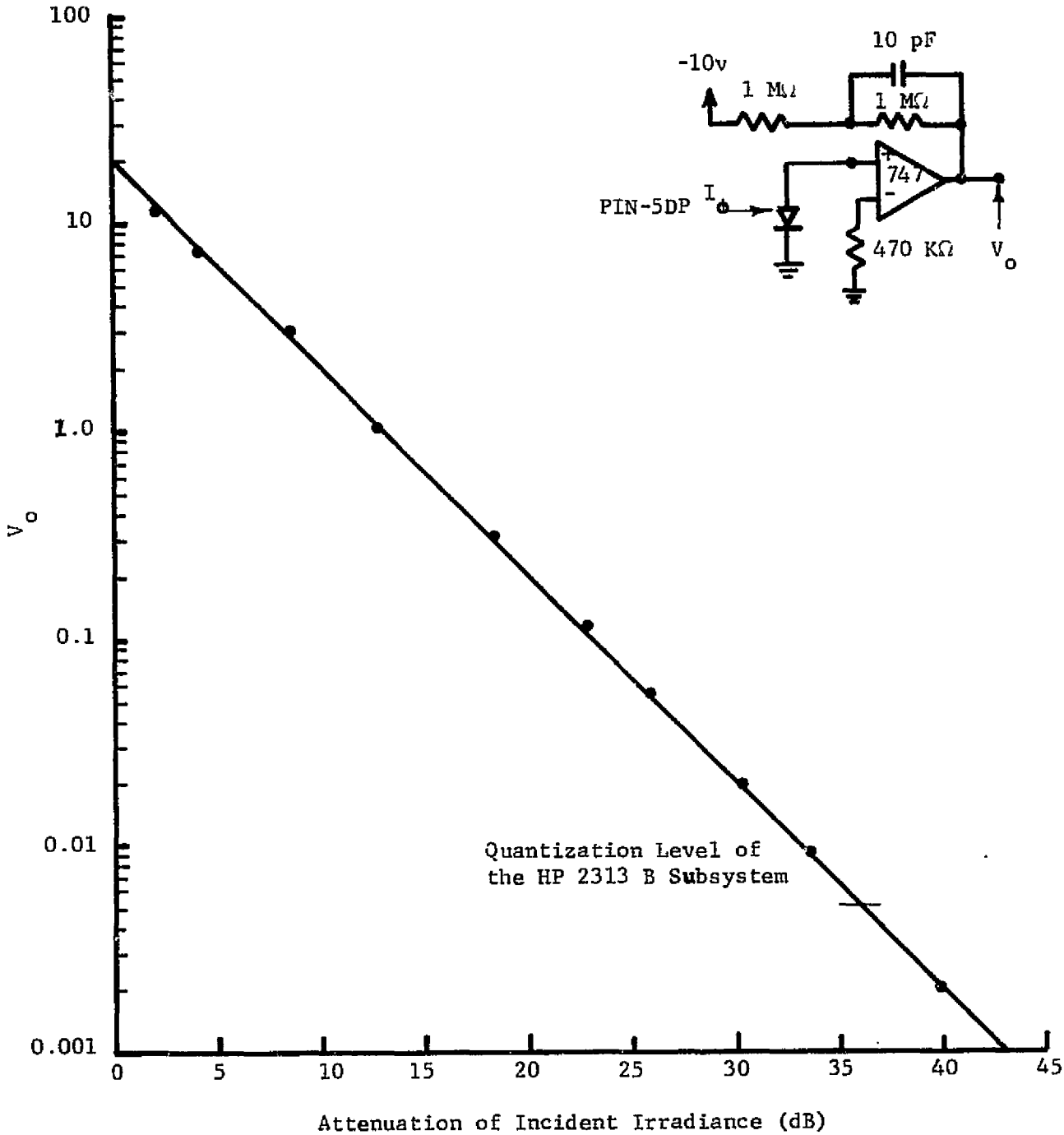


Figure 25. Linearity of the Photodetector-Operational Amplifier Pair.

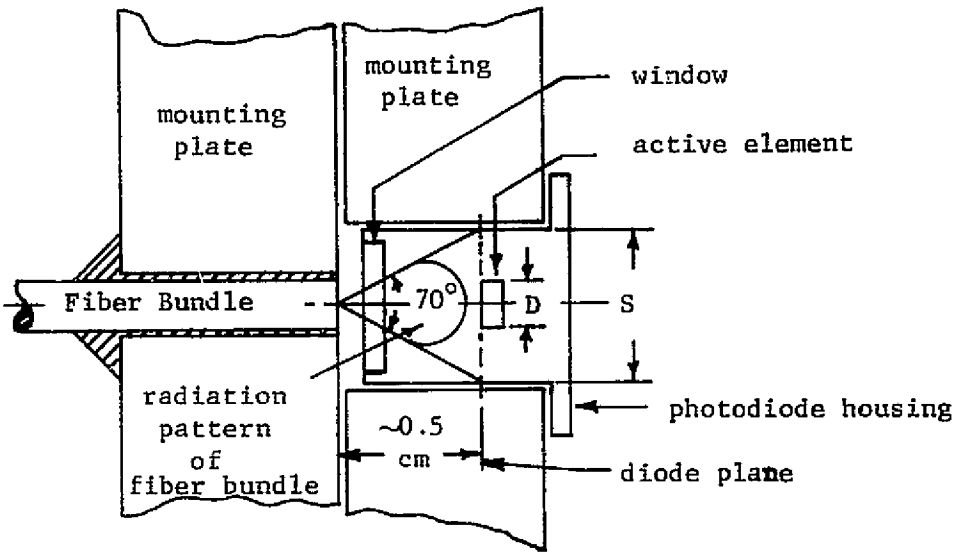


$$S \approx d_B + 2L\tan\theta/2 = d_B + 0.7$$

| Photodiode | Diameter of Active Element, D(cm) | Ring Number Assignments | Loss ($10 \log D/S)^2$) |
|---|---|---|---|
| 3 DP | 0.20 | 1 - 31 | 5.4 → 6.1 dB |
| 5 DP | 0.26 | 32 - 121 | 4.9 → 5.4 dB |
| 6 DP | 0.51 | 122 - 169 | 2.5 → 2.7 dB |

Figure 26. Geometry of Fiber Bundle - Photodiode Termination and Radiation Loss Calculations.

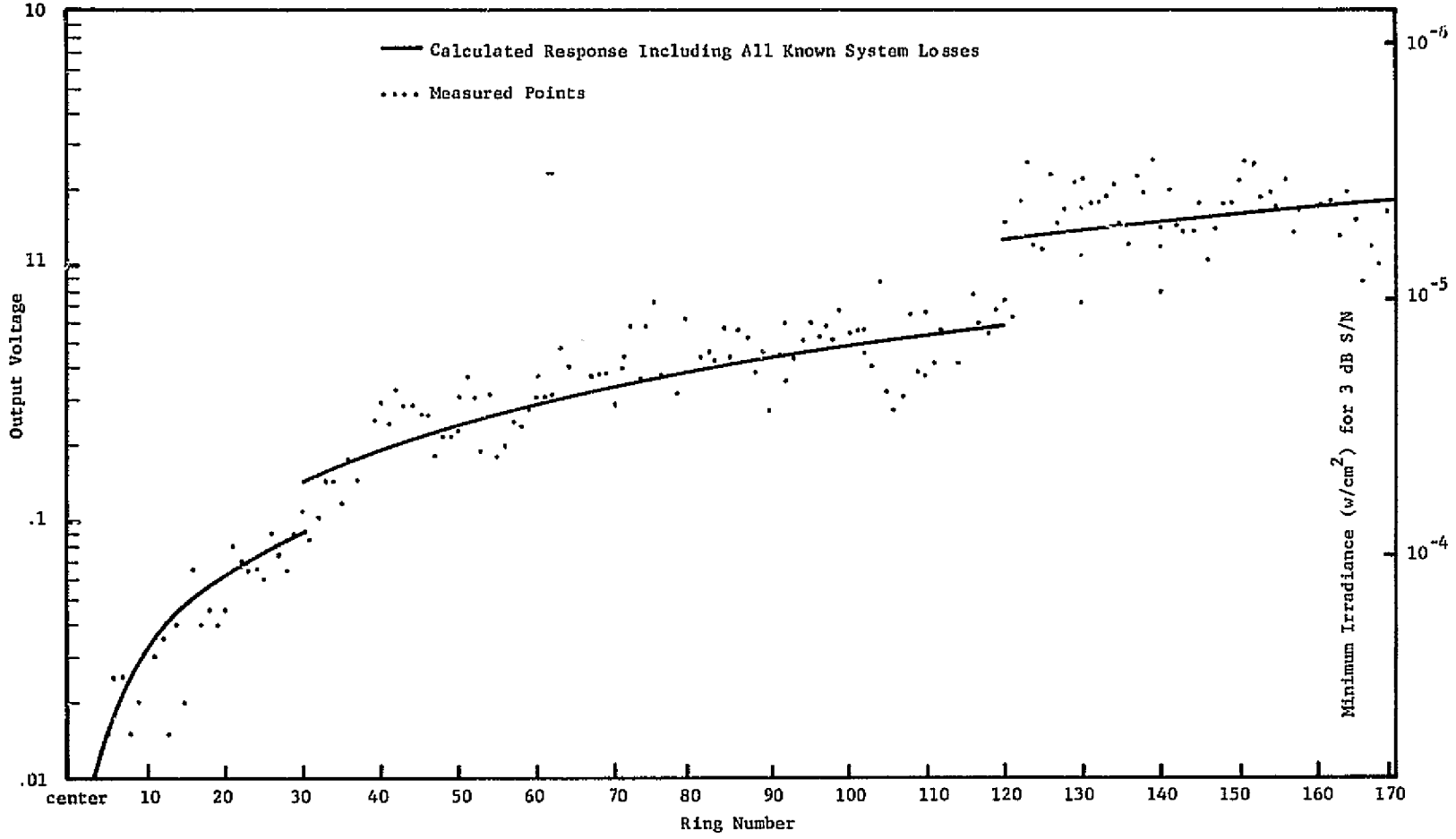


Figure 27. Radial Distribution Function of the Diffraction Pattern Sampling System.

measured points for the system characteristic are more widely distributed about the calculated characteristic than those for the fiber optic radial distribution shown in Figure 8. The wider distribution of points is a result of the spread in off-the-shelf photodiode sensitivities. A statistical analysis of the responses of the photodiodes incorporated into the system to an input irradiance of 190 $\mu W/cm^2$ is given below:

| Photodiode Type | Mean Output Voltage ($\bar{v}_o$) | % Standard Deviation ($\sigma/\bar{v}_o$ x 100) | % Maximum Deviation |
|---|---|---|---|
| 3 DP | 1.6371 | 17.3 | +37.4 - 41.4 |
| 5 DP | 2.7173 | 10.2 | +31.7 - 17.6 |
| 6 DP | 9.0688 | 21.2 | +74.2 - 29.4 |

Although the statistics of the operational amplifiers were not determined, a smaller spread in gain characteristics would be expected. No provisions were made to compensate for these variations in the electronics since dynamic changes can be expected to occur, and since these variations can be easily removed in the digital processing operations.

The sensitivity was determined by measuring the output signal-to-noise ratio for each channel under conditions of uniform illumination. These measurements are expressed in terms of the minimum irradiance as a function of radial coordinate for a 3 dB S/N at the HP 2313B output, and the minimum power incident on each photodiode for 3 dB S/N at the HP 2313B output. The minimum irradiance is given on the right hand ordinate of Figure 27, and the minimum power levels for the photodiodes are given below:

| Photodiode Type | $P_{min}$(w) for 3 dB S/N at the Output of the HP 2313B Subsystem |
|---|---|
| 3 DP | $9.73 \times 10^{-8}$ |
| 5 DP | $5.74 \times 10^{-8}$ |
| 6 DP | $2.60 \times 10^{-8}$ |

Although it is difficult to relate these sensitivity measurements to potential performance goals, certain criteria for the subject application can be suggested. The diffraction pattern of a low contrast image will be determined by its aperture function. If we assume that a 1 mm laser beam is used to scan aerial photograph (1 mm corresponds to $\sim$ 1 acre on the 70 mm imagery), the principle maximum of the diffraction pattern is contained within the first five rings for the present optical system parameters. The relative intensity of the remaining distribution, which contains the spatial information, is proportional to $m^2/4$, where m is the modulation index. For m = 0.5, the average irradiance of the information carrying spatial distribution is approximately $10^{-4}$ w/cm$^2$ for object irradiance of 3.8 w/cm$^2$. Assuming a 3 dB S/N, the required sensitivity is about $2 \times 10^{-5}$ w/cm$^2$. From this simple approximation, and the data of Figure 27 it is evident that the present system sensitivity is not adequate for low resolution spatial analysis. This conclusion was, unfortunately, found to be accurate when forestry diffraction patterns were recorded from the 70 mm aerial film.

The radiometric sensitivity of the fiber optic detector is affected by the cross coupling between adjacent rings. This is an especially important consideration near the center of the array where the undiffracted light intensity is much greater than that near the edges. To measure the magnitude of cross coupling, the spatial filtered and expanded laser beam (2 inch diameter) was projected through the Fourier transform lens and focused on the center fiber of the array. Precise centering of the focused spot was accomplished by observing the diffraction pattern in real time on the oscilloscope display of the digital processing system This centered distribution was then printed out on the teletype, and the cross coupling was determined from the light background corrected voltage readings. With careful alignment, it was found that the voltage on the first ring was 29.7 dB below the center fiber voltage, and that the voltage of all higher number rings was at the lowest quantization level of the HP 2313B A/D converter. Calculation of the diffraction pattern of a circular aperture of 2 inch diameter showed that the envelope of the intensity distribution for diffraction limited conditions would be about 45 dB

below the principal maximum at the radius corresponding to the first ring of the array. Thus it appears that the adjacent ring cross coupling level is about -30 dB, and that the dynamic range of the first ring would be reduced by only 6 dB. Since very little information will be contained in the low spatial frequency region, this performance level is satisfactory.

A potential system requirement that surfaced unexpectedly during the radiometric sensitivity tests should be mentioned because of its potential importance to pattern recognition processing. The argon laser used in these tests employs an internal light regulator, and according to manufacturer's specifications, the noise in a 10 Hz to 2 MHz bandwidth is $< 0.7\%$, and the long term amplitude stability is $< 1\%$ (1 sec. to 10 hours). During extended tests, the short term stability of the expanded and spatially filtered laser beam was observed to be about 10%. The stability for various intensity levels was measured, and found to be about the same. Interestingly, the stability of the unexpanded and unfiltered laser beam was measured, and found to be well within the specifications, with long term stability over several minutes below 0.5%. The degradation in stability was traced to two primary phenomena. The most serious problem was the poor vibrational isolation of the long optical path coupled with the positional sensitivity of the pinhole spatial filter. The presence of dust particles in the beam ahead of the spatial filter was also found to contribute to amplitude noise.

The stability was greatly improved by remounting the spatial filter, beam collimeter, and beam directing mirrors on short-stemmed, massive mounts, and enclosing the beam paths with plastic tubes to reduce the dust circulation. In addition, an external light amplitude feedback system was added to the laser by sampling part of the expanded and spatially filtered beam, and injecting a voltage proportional to the sampled intensity into the light regulator control loop. Without any attempt at optimization of this control loop, the short term stability and amplitude noise level was reduced to about 0.1%.

During processing operations, it will be necessary to impose amplitude stability requirements on the coherent source during the sampling interval

required for scanning the 169 photodiode outputs. The noise level of the laser beam will have to be at least 36 dB below the average intensity to utilize the full dynamic range of the A/D converters in the present processing scheme. Thus, the required noise and short term stability would be about 0.025%. Several alternatives to this requirement will be discussed in Section VI.

Operation of the digital processing system for analysis of the sampled diffraction patterns was described in Section IV, and the reader is referred there for details pertaining to operating procedures for the tests described in the following text. A photograph of the diffraction pattern sampling system is shown in Figure 28.

The accuracy of scaling between the object plane and the diffraction plane was confirmed by recording the diffraction pattern of a 250 line/inch ruled grating. A photograph of the diffraction pattern obtained by placing a film plate in the Fourier transform plane, and a photograph of the oscilloscope display of the optical processor is shown in Figure 29. The calculated and measured diffraction maxima of the 250 line/inch grating were found to be:

| CALCULATED MAXIMA | | | MEASURED MAXIMA |
|---|---|---|---|
| Diffraction Order | Radius (mm) | Ring Number (R(mm)/0.076+1) | Ring Number (from telecype print-out) |
| 0 | 0 | 1 | 1 |
| 1 | 2.88 | 38.8 | 39 |
| 2 | 5.76 | 76.6 | 76 |
| 3 | 8.63 | 114.3 | 115 |
| 4 | 11.51 | 152.1 | 152 |

Using the optical system parameters ($f = 23.58$ in, $\lambda = 1.921 \times 10^{-5}$ in.) and the measured spacing between the diffraction maxima as determined from the teletype print-out, the grating frequency was claculated to be 250.15 lines/inch. These measurements demonstrate the excellent accuracy with which object frequencies can be determined from the sampled diffraction patterns.

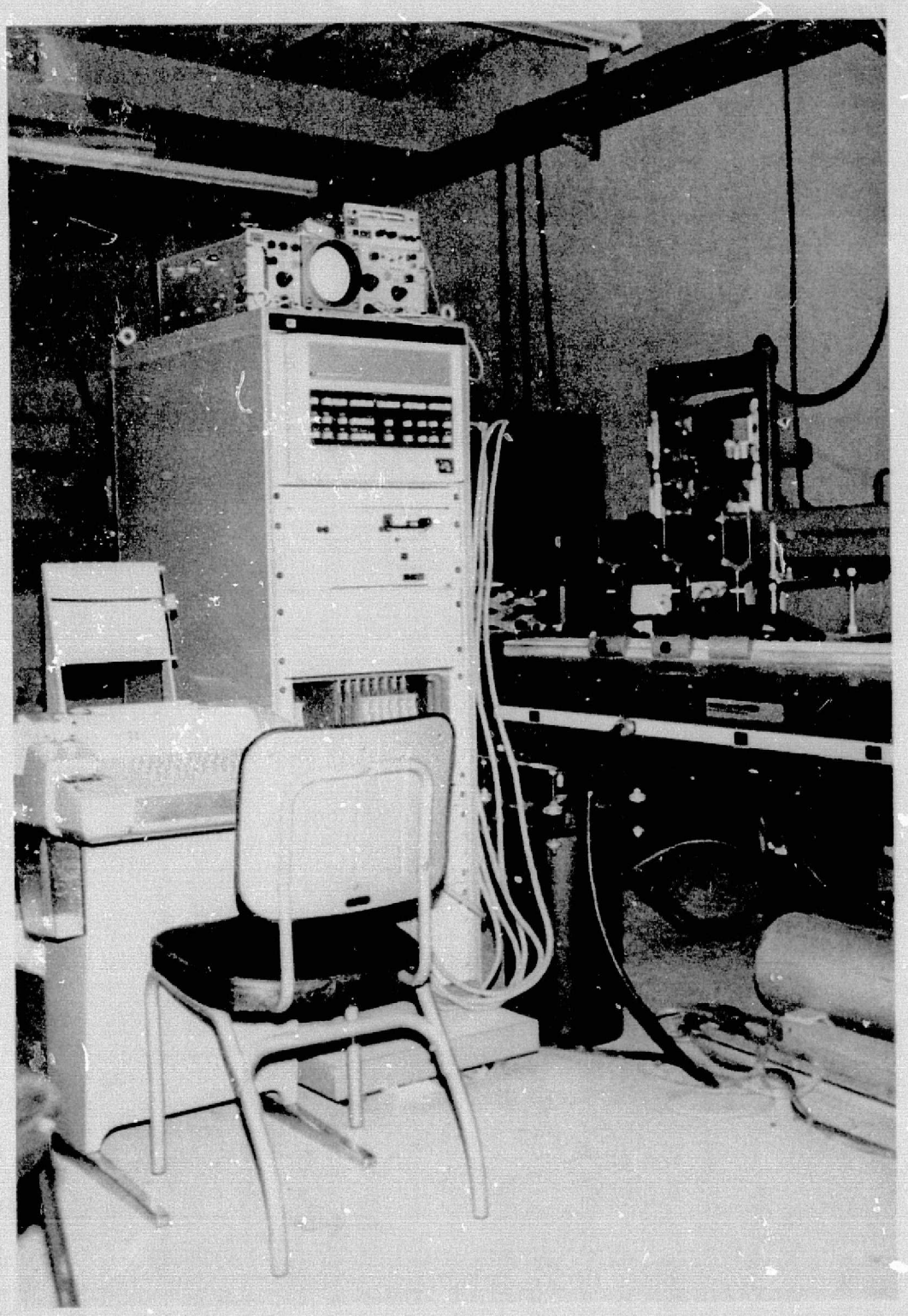

Figure 28. A Photograph of the Automatic Diffraction Pattern Sampling System.

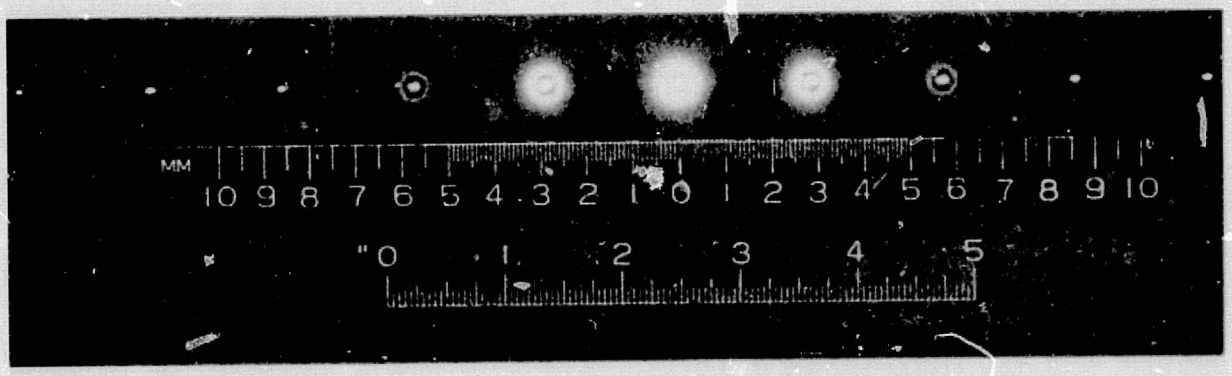


(a) Photograph of the Diffraction Pattern.

(b) Photograph of the Oscilloscope Display.

Figure 29. Diffraction Pattern and Automatic Diffraction Pattern Sampling System Display for a 250 Line/Inch. Grating Object.

A practical example of this type of analysis can be shown from Figure 30 which is a 20 power enlargement of a frame of the 70 mm aerial imagery taken over Huntsville, Alabama This photograph represents an area of approximately 2.6 x 3.2 miles located on the Redstone Arsenal, which includes a parallel array of roads and buildings located at about the middle of the frame. This grating like structure occupied an area of about 3.5 x 1.2 mm on the 70 mm film, and could be easily resolved with the unaided eye. Figure 31 shows a photograph of the Fourier transform diffraction pattern of the parallel structure of Figure 30 and its radial distribution function measured by the diffraction pattern sampling system. Three equally spaced diffraction maxima can be clearly seen above the background noise on the oscilloscope photograph of Figure 31. The grating spacing of the parallel structure was determined under a microscope, and the calculated and measured maxima are given below.

| | CALCULATED MAXIMA | | MEASURED MAXIMA |
|---|---|---|---|
| Diffraction Order | Radius (mm) | Ring Number (R(mm)/0.76+1) | Ring Number (from teletype print-out) |
| 0 | 0 | 1 | 1 |
| 1 | 1.21 | 15.9 | 16 |
| 2 | 2.42 | 31.8 | 33 |
| 3 | 3.63 | 47.7 | 49 |
| 4 | 4.85 | 63.6 | - |

The calculated and measured results are in excellent agreement in view of the relatively low accuracy of the microscopic measurements which were performed with the aid of an optical comparator.

As a final example of simple pattern recognition which is possible with grating like objects, consider Figure 32 which shows an enlargement from an aerial photograph of row crops, and the diffraction pattern of one of the cultivated areas. In this case, the rows could not be resolved on the original aerial photograph without enlargement, although the regular

Figure 30. Aerial Photograph of a Section of Redstone Arsenal.

ORIGINAL PAGE IS
OF POOR QUALITY

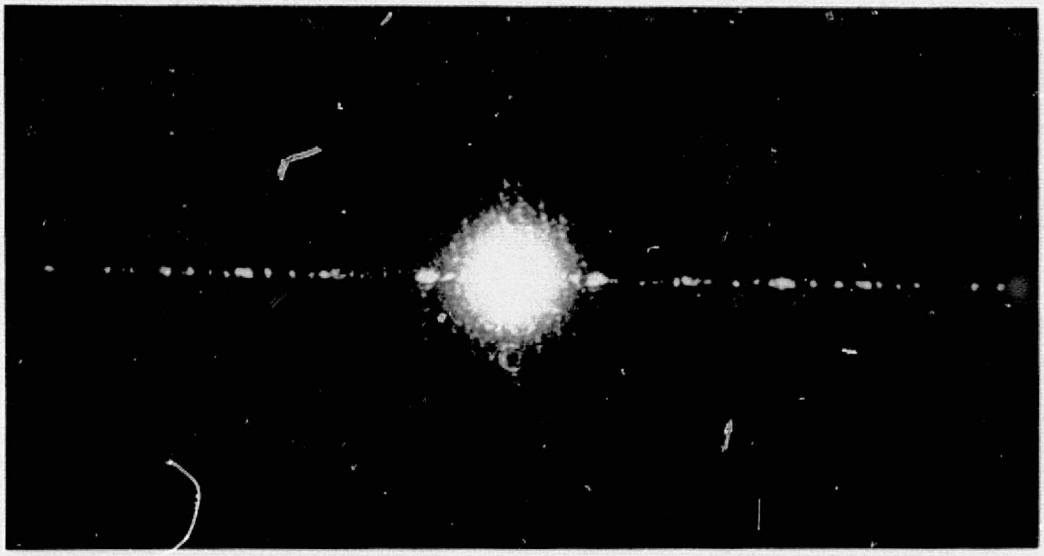

(a) Photograph of the Diffraction Pattern.

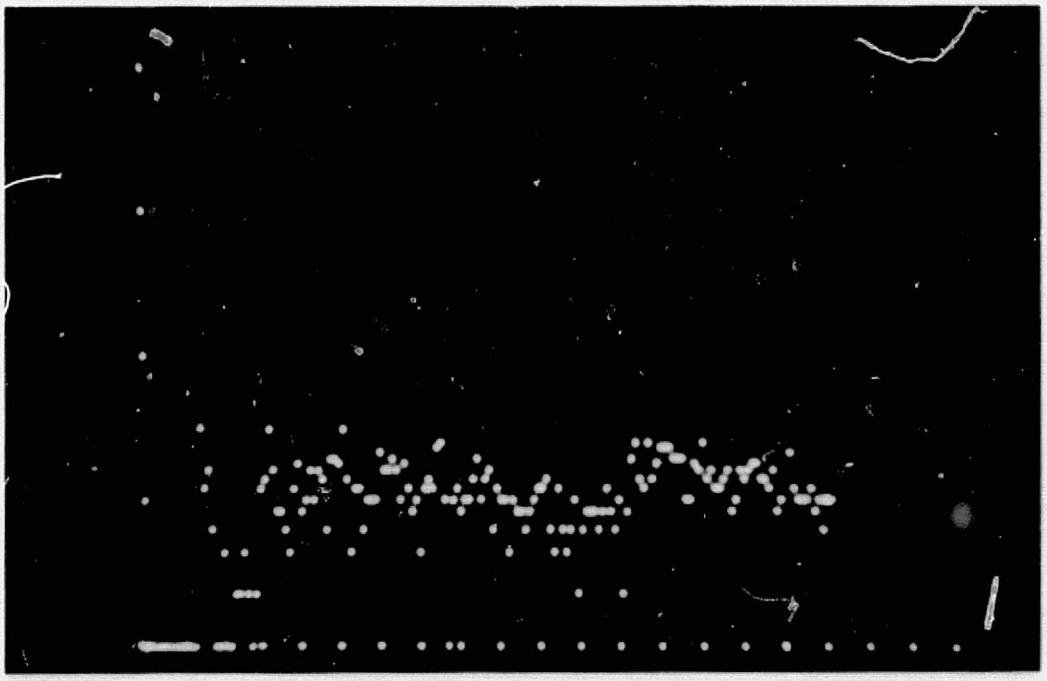

(b) Photograph of the Oscilloscope Display.

Figure 31. Diffraction Pattern and Automatic Diffraction Pattern Sampling System Display of a Parallel Line Structure on an Aerial Photograph of a Section of Redstone Arsenal, Alabama.

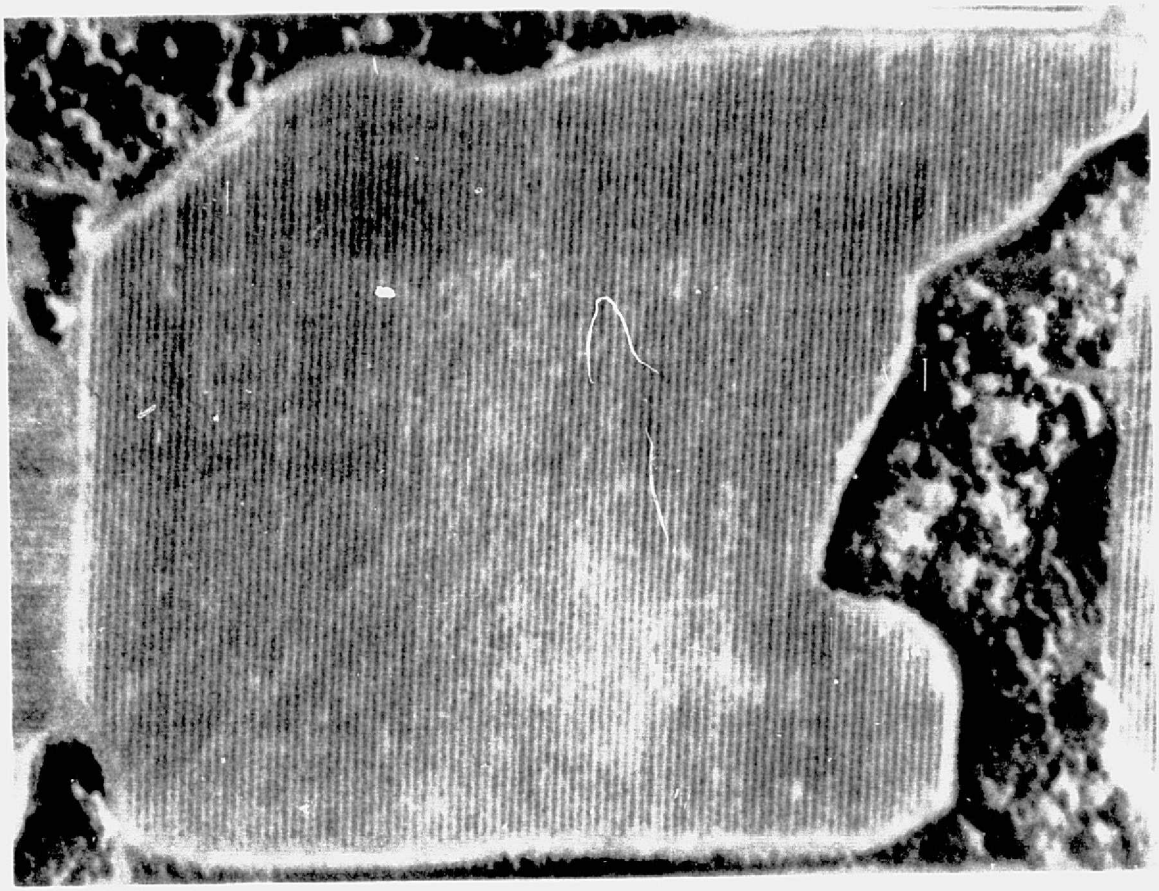

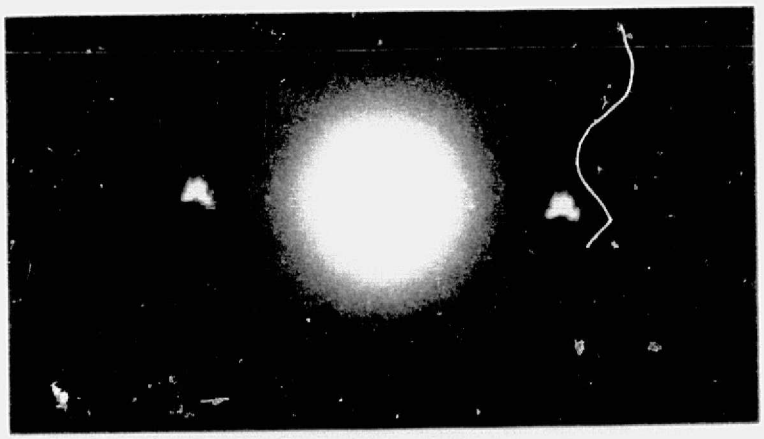

Figure 32. Enlarged Aerial Photograph of Row Crops and the Resulting Fourier Transform Showing Strong First Order Maxima.

spacing of this structure result in strong first order maxima which are easily recorded on the diffraction pattern sampling system.

Fourier transform diffraction patterns of other objects taken from the 70 mm film were recorded on the automatic diffraction pattern analyzer, but these objects did not yield signatures which could be readily analyzed with the present computer analysis programs. It is very likely that the resolution and contrast of the forestry images on the 70 mm film available for this study were not high enough to provide useable diffraction pattern signatures for the present system specifications.

# VI. CONCLUSIONS AND RECOMMENDATIONS

The goal of this program was to develop an automatic Fourier transform diffraction pattern sampling system, and to use this system to investigate techniques for forestry classification from six band multispectral aerial photography. The complexity of the system development resulted in the major effort being expended on development and testing of the system hardware. Software efforts were restricted to the generation of computer programs for sampling and recording accurate diffraction pattern representations under widely varying light background conditions.

The system parameters including sensitivity, dynamic range, spatial frequency resolution and adjacent ring cross coupling were measured, and system performance criteria based on these parameters were suggested. Performance tests with grating type objects showed that the system is capable of recognizing and accurately determining object geometries from the measured diffraction patterns. Further, these tests clearly showed the potential advantages of this system over photographic-densitometer techniques for optical pattern recognition.

In addition to establishing diffraction pattern sampling criteria, the system tests revealed several areas where improved electronic performance and changes in optical parameters would be advantageous. For example, maximum utilization of the highest resolution possible with cameras and films intended for aerial photography would require that the focal length of the Fourier transform lens be reduced from 59.89 cm to about 16 cm for a source wavelength of 488 nm. This change would result in the fiber optic detector encompassing at least two diffraction maxima for any barely resolved object. Improvement in the system sensitivity to accommodate diffraction pattern signatures of low contrast objects (such as forestry images) is also needed. An increase of about 5 dB in system sensitivity could be obtained by an improved photodiode mounting scheme which would reduce the fiber bundle to photo-diode element spacing. Beyond this relatively simple improvement, consideration should be given to incorporation of higher quality, low noise, operational amplifiers following the

photodiodes. Another interesting possibility would be to combine an additional electronic gain stage, possibly between the high level commutator and the A/D converter, with improved front end gain to vary the 36 dB dynamic range window up and down the absolute sensitivity scale. Finally, the requirements on laser amplitude stability for the present system sampling time interval were found to far exceed the capabilities of off-the-shelf laser devices. Howeve:, there appears to be several potential solutions for this problem. As discussed in Section V, an external feedback loop with the sample point in the expanded and spatially filtered beam would greatly improve amplitude stability. The error signal generated at this sampling point could also be injected into the reference voltage ports of the current-to-voltage converters in proper time sequence with the commutation operation. Still another possibility would be to record the error signal and perform the intensity adjustment in the digital processor. On the other hand, the requirements on amplitude stability would be greatly reduced if the 169 rings were sampled in parallel, and interrogated sequentially by means of sample and hold circuits following each of the operational amplifiers. These techniques and possibly others should be carefully evaluated to determine the optimum solution which would be both cost effective and satisfy the technical requirements.

The above system considerations apply to improvements in the accuracy of sampling and recording diffraction pattern signatures. It is imperative, however, that equal consideration be given to the development of effective algorithms for pattern recognitions processing. The system in its present state is suitable for preliminary development of processing operations for land use classification. A beginning step would be the investigation of art work photographic transparencies to determine the effects of contrast ratio and object shape on diffraction pattern signatures. At the same time, algorithms should be developed for recognitions of simple objects, and an investigation of the possible advantages of combining or weighting the outputs of the concentric rings electronically should be included.

Since spectral information is available from the aerial photographs at the undiffracted light location of the Fourier transform diffraction

pattern, careful consideration should be given to multiband processing techniques. A combination of spatial signature features plus spectral intensity would possibly provide a means for discriminating between different objects having similar shapes, and would lend itself to integration with well established digital processing techniques which are now applied to the analysis of multispectral earth resources data.

In summary, the power of optical processing in pattern recognition has long been recognized, but at the beginning of this program, methods had not been available for automatic sampling and processing of Fourier transform diffraction pattern signatures. A hybrid optical-digital system has been developed on this program as a first step toward the development of a real time optical processing system. Time and funding resources available to this program did not permit extensive development of algorithms for digital processing of the six band multispectral aerial photographs made available by MSFC for analysis. Test were performed and results were documented to reveal the accuracy for which Fourier transform diffraction pattern signatures could be sampled and recorded by the system developed on this program. These tests led to the identification of changes which should be made in the system hardware for improved diffraction pattern analysis. It is recommended, however, that the system in its present configuration be employed in a preliminary investigation of processing techniques for land use classification. Ideally system improvements and a study of processing techniques should be pursued concurrently. The initial steps for such a program effort have been outlined, and it is recommended that this program effort be continued toward development of an optical processing system for real time land use classification from a conventional aircraft or satellite platform.

## VII. ACKNOWLEDGEMENTS

The authors would like to acknowledge the technical contributions of Messrs. A. McSweeney and J. B. McManus to the optical systems measurements and analysis, the efforts of C. S. Wilson, Jr. in the design and fabrication of the optical-electronic interface, and R. D. Wetherington for assistance with the computer programming.

## VIII. REFERENCES


1. Lipson, S. G., and Nisenson, P., "Imaging Characteristics of the ITEK PROM," Applied Optics, 13, No. 9, pp. 2052-2060, Sept. 1974.
2. Shanks, I. A., "Liquid Crystal Materials and Device Developments," ELECTRONIC ENGINEERING, pp. 30-37, Aug. 1974.
3. Donjon, J., et al., "A Pockels-Effect Light Valve: Phototitus Applications to Optical Image Processing," IEEE Trans. Elec. Dev., ED-20, No. 11, pp. 1037-1042, Nov. 1973.
4. Smith, W. D., and Land, C. E., "Scattering-Mode Ferroelectric-Photoconductor Image Storage and Display Devices," Appl. Phys. Lett., 20, No. 4, pp. 169-171, Feb. 1972.
5. Lenduris, G. G., and Stanley, G. L., "Diffraction-Pattern Sampling for Automatic Pattern Recognition," Proc. IEEE, 58, No. 2, pp. 198-216, Feb. 1970.
6. Nyberg, S., et al., "Optical Processing for Pattern Properties," Photogrammetric Engineering, 37, pp. 547-554, 1971.
7. Gramenopoulos, N., "Finding the Earth in ERTS," Optical Spectra, pp. 26-28, Aug. 1974.
8. Feinleib, J., "Optical Processing in Real Time," Laser Focus, pp. 42-44, Sept. 1973.
9. Vander Lugt, A., "Coherent Optical Processing," Proc. IEEE, 62, No. 10, pp. 1300-1319, Oct. 1974.
10. Dobrin, M. B., "Optical Processing in the Earth Sciences", IEEE SPECTRUM, pp. 59-66, Sept. 1968.
11. McSweeney, A., "Design and Fabrication of an Engineering Model Fiber-Optics Detector," Final Report on Contract NAS8-28215, Georgia Institute of Technology, Dec. 1972.